Hindawi
International Transactions on Electrical Energy Systems
Volume 2024, Article ID 9196747, 25 pages
https://doi.org/10.1155/2024/9196747

Research Article

A Novel Hybrid MPPT Controller for PEMFC Fed High Step-Up Single Switch DC-DC Converter

Shaik Rafikiran,[1] **C. H. Hussaian Basha**,[2] **and C. Dhanamjayulu**[3]

[1]*Sri Venkateshwara College of Engineering (Autonomous), Tirupati 517507, Andhra Pradesh, India*
[2]*EV R&D Laboratory, NITTE Meenakshi Institute of Technology, Bengaluru 560064, India*
[3]*School of Electrical Engineering, Vellore Institute of Technology, Vellore, India*

Correspondence should be addressed to C. Dhanamjayulu; dhanamjayulu.c@vit.ac.in

Received 4 May 2023; Revised 7 February 2024; Accepted 29 February 2024; Published 12 March 2024

Academic Editor: Youcef Belkhier

At present, there are different types of Renewable Energy Resources (RESs) available in nature which are wind, tidal, fuel cell, and solar. The wind, tidal, and solar power systems give discontinuous power supply which is not suitable for the present automotive systems. Here, the Proton Exchange Membrane Fuel Stack (PEMFS) is used for supplying the power to the electrical vehicle systems. The features of fuel stack networks are very quick static response, plus low atmospheric pollution. Also, this type of power supply system consists of high flexibility and more reliability. However, the fuel stack drawback is a nonlinear power supply nature. As a result, the functioning point of the fuel stack varies from one position to another position on the V-I curve of the fuel stack. Here, the first objective of the work is the development of the Grey Wolf Optimization Technique (GWOT) involving a Fuzzy Logic Controller (FLC) for finding the Maximum Power Point (MPP) of the fuel stack. This hybrid GWOT-FLC controller stabilizes the source power under various operating temperature conditions of the fuel stack. However, the fuel stack supplies very little output voltage which is improved by introducing the Single Switch Universal Supply Voltage Boost Converter (SSUSVBC) in the second objective. The features of this proposed DC-DC converter are fewer voltage distortions of the fuel stack output voltage, high voltage conversion ratio, and low-level voltage stress on switches. The fuel stack integrated SSUSVBC is analyzed by selecting the MATLAB/Simulink window. Also, the proposed DC-DC converter is tested by utilizing the programmable DC source.

1. Introduction

From the present literature survey, the availability of Nonrenewable Energy Resources (NESs) is decreasing extensively because of its disadvantages such as high catchment area for the installation, more environmental effects, a high effect on the ozone layer, direct effect on human life, and more power generation price [1]. In addition, this type of power system is not suitable for rural areas. So, the current research is focusing on the RES for supplying the energy to all local as well as urban people. The classification of RES is wind, geothermal energy, ocean energy, hydropower, solar energy, and bioenergy. In article [2], the authors discussed the wind power supply networks for generating electricity in the coastal regions. In this wind network, the modern turbines with very low specific ratings plus high hub heights increase the wind energy potential. As a result, the overall wind power system installation cost is reduced [3]. Here, the wind turbines capture the wind velocity for running the dual-fed induction machine. The major problem of wind power systems is noise creation by wind turbines which may not be accepted by human beings [4]. Especially, birds and bats are seriously affected by the wind power network. Also, the main challenge of the wind system is the minimization of levelized production costs. Levelized production cost of the wind system is decided based on the energy production cost concerning the economic life time of the utilized system [5]. Finally, the wind systems are installed in limited places because of the potential impact on the environment.

All of the wind systems' drawbacks are limited by utilizing the geothermal power supply networks. In these geothermal systems, the fluids are collected from the

underground reservoirs and it is used for the conversion of water into steam. The generated steam is sent to the turbines to run the electrical machine [6]. In the literature, there are various types of geothermal power networks available such as flash steam, dry steam, and binary cycle. Here, the type of power conversion depends on the power plant design which is mainly focused on the fluid surface and its operating temperature. The dry steam power plant takes hydrothermal fluids which are closely available in the form of steam [7]. In this system, the available steam is directly sent to the rotating turbine which is directly coupled with the functioning generator for supplying the peak power to the emergency applications like shopping malls and hospitals. The dry steam power plants are a very old type of power plant that was first referred to by Lardarello in the nineteenth century. Similarly, the flash type of power network is a commonly used power network that collects the fluids with high functioning temperatures [8]. Finally, the binary cycle geothermal power network is used for supplying power to the local consumers at low as well as high fluid operating temperature conditions [9]. The merits of geothermal systems are low-level environmental pollution, moderate sustainability, massive potential, and more reliability. However, the disadvantages of geothermal systems are minor environmental pollution, suitable for a specific location, mostly preferable for urban areas, and high initial cost [10].

The demerits of geothermal systems are limited by using ocean energy systems. In this ocean energy, the wave energy is captured by using the turbines and is transferred into the electrical power supply by using the bidirectional electrical machines. The features of ocean energy systems are nature-free, unlimited availability, high potential, good reliability, and zero environmental pollution. The demerits of this system are high installation cost and need for high scalability. In addition, the urban areas will benefit from the help of the ocean energy system. The limitations of ocean energy systems are overcome by using the hydropower networks [11]. From the literature review, there are different types of hydraulic systems available in nature and all of these systems utilize the kinetic energy of water flow from upstream to downstream. Here, high-pressurized storage water is utilized to achieve the kinetic energy of the water. The features of hydrosystems are useful for peak load demand, nonpolluting sources of energy, more resilience, and low distribution power cost [12]. However, the drawbacks of hydrosystems are limited by utilizing solar power systems. From the literature review, sunlight energy is available in nature excessively free of cost. Here, the sunlight insolation comes to the earth with different incident angles. The solar photovoltaic panels are installed on the earth in such a way that the incident angle of sunlight irradiation is exactly perpendicular to the PV panel [13]. Once the PV panel receives the sunlight insolation energy, the free electrons in the P-N type materials of the PV absorb the sun energy and start functioning to generate the electrical power supply [14].

The working behavior of the PV is exactly similar to the normal P-N diode operation. Solar cells are developed by utilizing the various categories of advanced manufacturing technologies which are named thin film, polycrystalline, and monocrystalline. The thin film-based solar cells have various types of advantages when compared to the 1st generation silicon solar cells in terms of lighter weight, thin construction, and more flexibility [15]. Due to these merits, the thin film model solar systems are utilized in integrated residential buildings and water heating systems. In [16], the authors utilized the polycrystalline model solar cells for the large-scale solar power network installation. Here, there are multiple crystalline solar cells involved in each polycrystalline model solar panel. As a result, polycrystalline solar cells work at very low functioning temperature conditions of the sunlight system. These types of solar cells are used in large-scale commercial buildings for supplying electricity to consumers [17]. So, most human beings are independent of the central grid for power consumption. However, thin film and polycrystalline solar cells have drawbacks such as low sunlight energy conversion efficiency, being less suitable for domestic application, and being moderately expensive [18]. So, monocrystalline silicon solar panels are utilized in most places because their merits are more efficiency, crystal structure, and more reliability. However, these solar modules require high implementation costs and less power production under high operating temperature conditions of the solar systems.

Each solar cell voltage production is 0.95 V to 1 V which is not at all useful for any local consumers. So, the solar modules are series connected to enhance the voltage capability of the overall system. Sometimes, the peak loads require a high number of currents; then, the solar modules are placed in a parallel fashion [19]. So, multiple types of solar cells are connected in parallel plus series for supplying the power to the electric vehicle applications. The major issue of solar systems is discontinuous power supply and less useful for industrial applications. So, in this article, the fuel stack technology is utilized for the four-wheeler system for the continuous functioning of the electric vehicle network. Here, the fuel modules are differentiated based on the usage of electrolytes in the system. The fuel modules are classified as Alkaline Fuel Module (AFM), Molten Carbonate Fuel Module (MCFM), Regenerative Fuel Module (RFM), Proton Exchange Membrane Fuel Module (PEMFM), Phosphoric Acid Fuel Module (PAFM), and Solid Oxide Fuel Module (SOFM). The alkaline fuel network is utilized in the article [20] for supplying the rated voltage to the microgrid network. Now, the microgrid is gaining a lot of attention. The microgrid involves the battery charging station, fuel stack, and various renewable energy systems [21]. All the power supply networks are interfaced to one common busbar for maintaining the constant load voltage. Here, the alkaline model fuel network supplies heat combined with water and electrical power supply by utilizing the inputs oxygen plus hydrogen chemical decomposition. In this fuel stack, the electrode is placed in between the anode material and cathode material and it is manufactured by selecting the alkaline membrane [22].

The merits of an alkaline fuel stack network are moderate efficiency, very simple heat management, moderate startup time, high chemical activity, and less expensive anode and cathode materials. In addition, the internal combustion of an

alkaline network is easy when equated with the battery system [23]. As a result, the fuel stack takes less money for power supplying to the global industries. Especially, the alkaline fuel stack networks are more useful for saving labor time and less installation space and are more suitable for peak load application. The main applications of alkaline fuel stacks are backup power supply, highly useful for commercial and residential building applications [24]. However, the alkaline fuel stacks are very intolerant to carbon dioxide because CO_2 consumes more alkaline chemical decomposition. As a result, the overall system chemical reaction and operating system efficiency are reduced extensively. The demerits of alkaline fuel cell modules are limited by applying the reversible fuel stacks. In these reversible fuel stacks, the input hydrogen fuel is obtained from pure water [25]. Here, the water is split into hydrogen and oxygen ions by using other renewable energy systems like wind and solar systems. On the other hand, the reversible fuel stack gives heated steam which is again fed back to the power supply system by converting into water. This type of fuel stack network is more popular for emergency power supply applications. The disadvantages of reversible fuel stacks are compensated by applying the molten carbonate fuel module.

In this MCFM, the alkali metal carbonate electrolyte is used and its maximum functioning temperature capability is 650°C. Due to this high operating temperature, the selected input fuel for the MCFM is directly fed to the electrolytic channel for generating the electrical power supply with high operating efficiency [26]. The selected input chemicals to the MSFM are carbon dioxide, hydrogen, and oxygen, and the heated water is released from the output of the fuel stack. The MCFM advantages are high operating pressure, less reversible, and good output power conversion efficiency. However, this fuel stack is not suitable for portable applications and needs sealing [27]. So, the proton exchange membrane fuel module is used in this work for supplying power to the electrical vehicle systems. This fuel stack can work at very low as well as high operating temperatures. The major features of this PEMFM are compact design, high-energy density, and maximum values of specific power per unit and volume. In addition, its starting speed is very high when equated with the other fuel cells. The present demand for fuel stacks is illustrated in Figure 1, and the types of fuel stacks are represented in Table 1.

All the fuel stack disadvantages are continuous variations of power due to the continuous variation of the functioning point of the fuel stack. So, there are different categories of Maximum Power Point Tracking (MPPT) methodologies used in the literature to stabilize the functioning point of the fuel stack which are machine learning algorithms, optimization technologies, soft computing, nature-inspired algorithms, and conventional controllers. In [29], the researchers applied the Perturb & Observe (P&O) conventional controller to identify the working point of the fuel stack interfaced bidirectional three-phase power converter. Here, initially, the working point of the fuel stack is identified on the V-I curve of the system. Suppose the identified functioning point of the fuel stack is on the left side of the V-I curve and then the equivalent resistance of the source system is modified by enhancing the operating duty cycle of the converter. Otherwise, the equivalent resistance of the overall system is reduced to move the working point of the fuel stack to the actual MPP position [30]. The general merits of this controller are simple in design, less implementation cost, easy to install, and less manpower requirement. However, this controller gives more steady-state fluctuations. As a result, the overall system gets vibrated. All the renewable energy-based power converters create fluctuated voltage and power. In the Kalman filter concept, the available voltage ripples and power ripples are fed to the Kalman filter block for suppressing the fluctuations of fuel stack output power. This controller identifies the functioning point of the renewable energy system by utilizing the ripples of the voltage and power [31]. So, it does not require any additional filters. Due to this condition, the overall system installation and manufacturing costs are limited. However, this controller is useful for only constant operating temperature conditions of the fuel stack.

For fluctuated temperature conditions of the fuel stack, the researchers are referring to the nature-inspired power point tracking controllers. In this work, the grey wolf optimization technique involves an adaptive fuzzy logic controller developed for enhancing the power conversion efficiency of the fuel stack [32]. The merits of this proposed nature-inspired hybrid MPPT controller are less level of dependence on fuel stack modeling, very good dynamic response, more suitable for all types of operating temperature conditions of the fuel stack, high tracking speed, fast convergence ratio, and useful for continuous peak load conditions. However, another issue with the fuel stack is the very high supply current [33–36]. If the fuel stack is directly interfaced with the battery, then the overall network power supply conduction losses are increased. Due to that, the entire system's functioning efficiency is reduced. From the literature survey, the power converters are applied to the electric vehicle systems to optimize the fuel stack output supply current. The power converters are differentiated based on the utilization of transformer and rectifier circuits. The transformers including power converters are feedforward, push-pull flyback, and bridge-type converter. Here, isolation means the separation of the source with a converter device to protect the overall network from overvoltage [37]. The merits of isolated power converters are strong anti-interference ability, easy-to-achieve multiple outputs, easy conversion of buck and boost operation, more security, and fewer possibilities of load damage. Also, these converters are useful for wide input voltage operation [38]. However, the isolated power converter networks have many disadvantages which lead to very low power transformation efficiency, relatively very large volumes, more expensive, and very high design complexity. So, the current industry is focusing on the transformerless power converters which are buck-boost, Cuk, and Luo converters [39]. However, these fundamental power transformation circuits have the disadvantage of less power transmission efficiency and are moderately suitable for peak load conditions [40, 41]. So, in this article, a Wide Supply Voltage Power Converter Circuit (WSVPCC) is

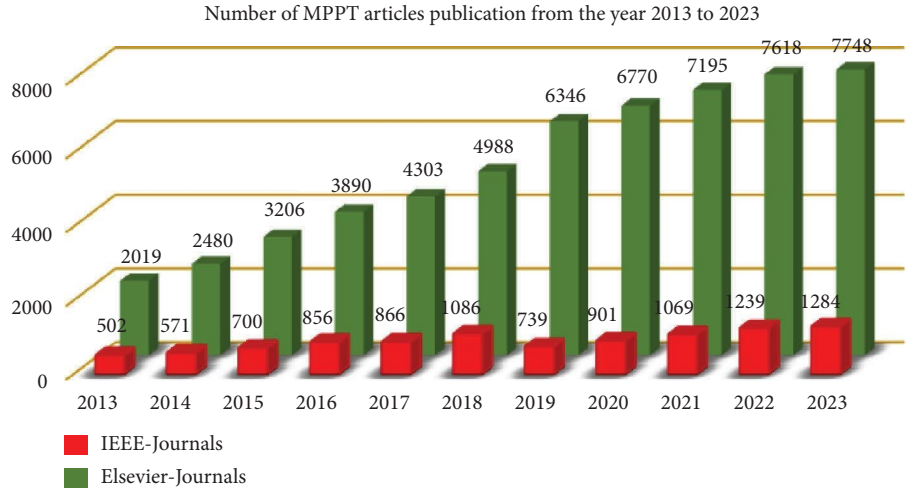

Figure 1: Latest trend of fuel stack utilization in different years [27].

proposed to reduce the fuel stack output current and improve the supply voltage profile of the overall system. The proposed power converter fed power point identifier is shown in Figure 2. From Figure 2, the power converter gives high voltage gain, low output voltage fluctuations, and very little current and voltage stress on power switches. In addition to that, this converter takes very little space for installation and its manufacturing cost is also reduced.

2. Literature Review on Past Published Works

From the literature review, the past isolated power converter circuits needed more implementation cost and needed more reliability. Also, these converter topologies require high installation space. So, transformerless power converter circuits are developed in [42] for battery charging systems with the help of solid oxide cells. The basic buck converter circuit is utilized in the PV/fuel stack microgrid system for balancing the power in the all-distribution loads. These converters required only one capacitor, plus one switch for balancing the supply voltage. Similarly, a simple boost converter circuit is applied in a telecommunication network for solar battery charging, plus discharging. The general boost converter circuit required less manufacturing cost, was easy to handle, and needed very low space for installation. However, these types of power converter circuits give less efficiency for high switching frequency applications. In [43], the authors worked out the hybrid electric vehicle technology to reduce the dependency on fuel engines. The combustion engine is interlinked with the electric drive network for regulating the power of the vehicle at various working temperature conditions of the fuel engine. The hybrid EV network's overall efficiency depends on the electric vehicle powertrain.

In EVs, the permanent magnet machine is utilized along with the battery for running the EV at constant speed. In [44], the solid oxide fuel stack network is merged with the quasi-source DC-DC converter topology and it is applied to the four-wheeler electric vehicle system to improve the efficiency of the system. In SOFS, the electricity supply process happens by utilizing the ceramic electrolyte [45]. Here, the negative oxygen ions flow from the cathode layer to the anode layer via a ceramic electrolyte. The analysis and the specifications of various categories of fuel stacks are explained in Table 1. In the SOFS, there is a high level of chemical decomposition happening at high operating temperature conditions of the fuel stack. As a result, the performance efficiency of the overall system is improved. Also, it consists of high fuel flexibility, less carbon dioxide emissions, and a relatively very low cost of implementation when compared to the phosphoric acid fuel cell [46]. The interleaved single-phase power electronic circuit topology is applied for the high voltage rating battery-based fuel stack system for running the battery in a dual power flow direction at peak load conditions. The lithium-ion battery state of charge and the state of discharge parameters are supplied to the incremental resistance MPPT block for optimizing the discharge state of the battery. In this MPPT methodology, the variation of fuel stack voltage and current variables is utilized for finding the duty ratio of the bidirectional power converter [47]. Here, the incremental resistive value is positive when the controller reaches the required MPP place. Otherwise, it may go to the left side of the MPP position of the fuel stack V-I curve.

The modified slider methodology is utilized in the hybrid diesel engine, battery, and fuel stack system for identifying the peak power point of the fuel stack, plus enhancing the dynamic response of the overall network [48]. In this power production network, the interleaved multiphase power converter is utilized for equal power distribution to all local loads. In this slider controller, the fuel stack oxygen ions, resistive load voltage, and hydrogen decomposition constants are utilized as the state input variables, and the output variable is the switching signal to the fuel stack-fed rectifier circuit [49]. All the rectifiers generate fluctuated currents and voltages which are given to the Kalman filter block for mitigating the losses of the hybrid PV/fuel stack network. The merits of this slider MPPT method are very easy, plus good static response. Also, it helps to optimize the fuel stack system power conduction losses. However, this slider controller may not give efficient converter output power. The demerits of this slider controller are overcome by using Artificial Neural Networks (ANNs) [50].

Table 1: Detailed illustration of various categories of fuel stacks [28].

Stack technology	PEMFSM	AFSM	PAFSM	MCFSM	SOFSM
The chemical applied in the fuel stack	Ions of hydrogen	Ions of hydrogen	Ions of hydrogen	Ions of hydrogen	Carbon monoxide H_2
Chemical composition	Pure air and O_2	Pure air and O_2	Pure air and O_2	Pure air and O_2, CO_2	Pure air and O_2
Applied electrolyte category	Polymeric	KOH	H_3PO_4	Molten carbonate	$CaTiO_3$
Maximum withstanding (T)	From 62°C to 84°C	From 73°C to 202°C	220°C–225°C	Highest of 622°C	Highest of 968°C
Rated available power	From 1 kW to 273 kW	From 7.8 W to 97.9 kW	From 44157 W	334 kW–1.8 MW	1 kW to 2 MW
Efficiency of cell	From 58% to 64.6%	From 56% to 61.5%	From 34% to 39%	47.7%–56%	47.77%–59.55%
Applications of the fuel stack	Battery-operated networks, plus electric vehicles	Apollo series space machines, plus hotels	Schools, office buildings, and manufacturing centers	Natural gas, coal-based power networks, and military	Stationary power supply, plus high-power EVs

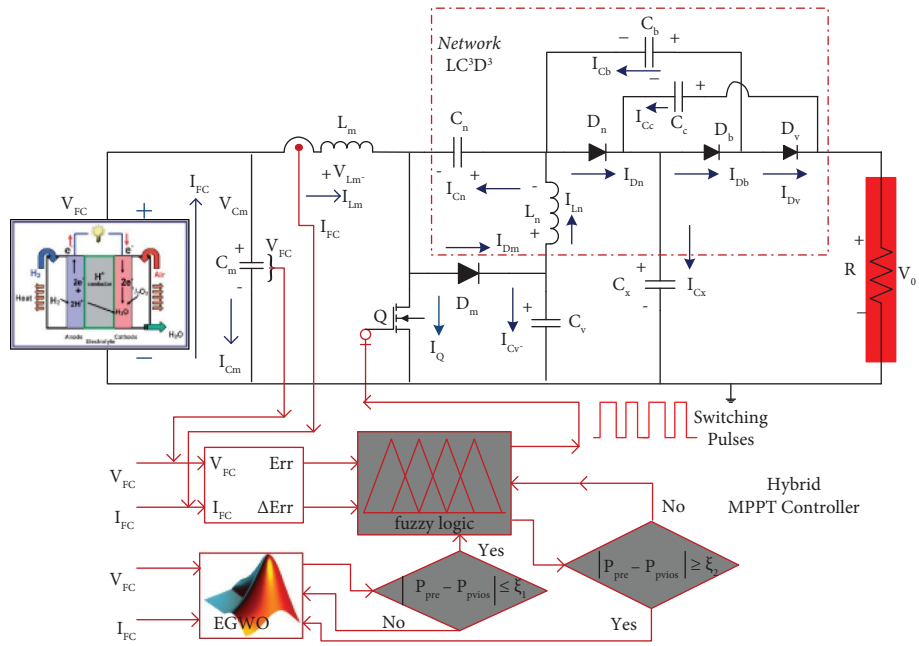

Figure 2: Grey wolf optimized adaptive fuzzy MPPT controller fed WSVPCC for fuel stack application.

The ANN controller is developed from the human brain's behavior and the human brain consists of multiple nodes that are interlinked with each other [51]. All the nodes are exchanging their information to identify the required objective. In [52], the PEMFS/battery-fed bidirectional power conversion circuit duty signal is monitored with the help of a neural network-based MPPT controller. The merits of these neural networks are very low implementation cost, more useful for all nonlinear issues, ease of use for highly complex problems, and the capability to alter any unknown conditions [52]. However, these neural networks need high convergence time, plus more complexity in the ANN structure. The feedforward neural network is utilized in the diesel/battery/PEMFS system for controlling the converter duty signal at various atmospheric conditions of the fuel stack [53]. A detailed analysis of different types of MPPT controllers is given in Table 2.

3. Design and Performance Study of Fuel Cell

As we know nonrenewable power system utilization is reducing drastically in electric vehicle systems because of its demerits such as large space for installation, plus high-power generation cost [59]. So, renewable power systems are playing the predominant role in the present electric vehicle systems for optimizing environmental pollution and reducing grid dependence. From the literature study, there are different types of renewable power systems available in the society. However, most of the renewable power supply networks give discontinuous power supply. So, in this work, the fuel stack technology is referred for continuous power supply to the automotive systems. In [60], the researchers studied the phosphoric acid fuel stack-based microgrid network for giving energy to local consumers. In this microgrid, the PV/wind/fuel stacks are involved in storing the energy in batteries, and the stored energy is utilized for emergency applications. In PAFSM, the phosphoric liquid is utilized as an electrolyte, and it is highly tolerant to carbon monoxide and carbon dioxide [61]. In addition, it is pollution-free and eco-friendly. The PAFSM is very less sensitive to CO_2 and it has the capability of regeneration of heat along with electricity. Finally, the phosphoric acid fuel network consists of very low volatility. In this fuel stack, the anode accelerates the hydrogen oxidation reaction rate in phosphoric acid. In this fuel stack, the anode must and should be stable for high operating temperature conditions of the phosphoric acid. Sometimes, hydrogen starvation happens in the PAFSM and then the anode gets affected by reverse polarization. However, this fuel stack is inherently much less powerful when compared to the other fuel cells [62].

The demerits of the phosphoric acid fuel stack are limited by using the solid oxide fuel cell. In the SOFSM, the natural gas flows through the steam reforming process for generating electricity [63]. Here, the methane and oxygen chemical recombination generates carbon monoxide, carbon dioxide, water, and hydrogen. The merits of solid oxide cells are high-functioning efficiency, long-term stability, fuel flexibility, less emission, relatively low cost, and low environmental pollution. The biggest disadvantage of SOFSM is taking more time to start functioning. However, the demerits of SOFSM are limited by using the polymer membrane fuel stack. In this PEMFSM, the proton ions are transferred from the anode chamber to the cathode chamber via a polymer electrolyte. Here, the membrane structure is in the form of a thin plastic film and it is permeable with the proton when the membrane is saturated with water. However, it may not conduct with the electrons. The working block diagram of the polymer membrane fuel stack and its corresponding functioning circuits are illustrated in

Table 2: The detailed investigation of various power point identifiers for PEMFS-fed DC-DC converter.

Authors	Available year	Utilized variables	MPPT	Obtained signal	Utilized DC-DC converter	Major findings
Karthikeyan et al. [54]	2021	Temperature, V_{FC}, and O_2	Feedforward ANN	Duty cycle	Ultra-high step-up converter	The feedforward ANN controller is applied to the 1.26 kW rated fuel stack to achieve the peak power from the overall system at various operating temperature conditions of the fuel stack. In this controller, the backpropagation methodology is utilized to activate the neural network controller.
Nureddin et al. [55]	2020	Hydrogen, temperature, and PV current	Deep neural network	Duty cycle	Bidirectional converter, and inverter	In this article, the electricity demand is illustrated in detail how it is increasing in an ascending manner. Conventional power systems are not useful to consumer demand. So, the fuel stack and PV sources are combined with the present available conventional sources to increase the availability of power to the consumers under different environmental conditions.
Kiran et al. [56]	2022	Temperature, PEMFS voltage	Radial basis function	Duty cycle	Single switch boost	Conventional neural networks may not be suitable for hybrid PV/battery networks because of their lower working efficiency under various atmospheric temperature conditions. The radial basis functional neural network is utilized in this power supply network for the improvement of the convergence speed of the MPPT controller. The merits of this controller are more efficiency and less training data.
Hai et al. [57]	2022	Oxygen pressure, PEMFS voltage	Adaptive neuro-fuzzy inference system (ANFIS)	Duty cycle	Buck-boost	Most of the fuel stack works long lifetime duration when equated with the battery, and it works sufficiently with high operating efficiency. However, these systems do not give the linear response for peak load industrial applications. So, the ANFIS methodology is utilized in this network for running the operating point of the fuel stack near the actual MPP. The algorithm is monitored by applying the modified fluid search algorithm.
Abou Omar et al. [58]	2019	Temperature, fuel stack voltage	Fuzzy with proportional and integral	Duty cycle	DC-DC boost converter	In this work, the neural network concept is utilized for the optimization of fuzzy membership rules. The proportional controller is interfaced in the fuzzy network for modifying the MPP location of the fuel stack system. The integrator in the controller helps to remove the dynamic oscillations of the overall system.

Figures 3(a) and 3(b). From Figure 3(a), in the cathode chamber, the protons are reacted with the electrons, and oxygen for generating the heat, and water are the by-products. In this fuel stack, the single cell voltage is defined as V_{FC} and in this stack are "N" number of cells are utilized for meeting the peak load demand voltage (V_{0L}). From Figure 3(b), the variables R_{0L} and R_{AL} are the ohmic power loss of the electrode plus active region power loss of the electrode. Finally, the term R_{CL} is identified as concentrative power loss of the fuel stack. The related voltages of the fuel stack are represented as V_{0L}, V_{AL}, and V_{CL}. The generated power and voltage curves are illustrated in Figures 4(a) and 4(b). The term T_F is the functioning temperature of the fuel stack. The partial oxygen pressure and hydrogen pressure are identified as P_{O2} and P_{H2}. The anode humidity vapor pressure and cathode humidity vapor pressure are identified as RH_{Ap} and RH_{Cp} and its related internal pressures are P_{Ap} and P_{Cp}. The water pressure and current flowing through the electrode are represented as $P^{sat}_{H_2O}$ and I_S. The utilized electrode area and empirical coefficients are defined as A, z_1, z_2, z_3, and z_4. The design constraints of the utilized fuel stack are shown in Table 3.

$$H_2 \Rightarrow 2H^+ + 2e^-, \tag{1}$$

$$2e^- + \frac{1}{2} O_2 + 2H^+ \Rightarrow H_2O, \tag{2}$$

$$\frac{1}{2} O_2 + H_2 \Rightarrow H_2O + \text{Energy}, \tag{3}$$

$$V_{OL} = N * V_{FC}, \tag{4}$$

$$V_{FC} = V_{OL} - V_{OL} - V_{AL} - V_{CL}, \tag{5}$$

$$V_{OL} = 1.905 - 0.779e^{-3}\left(T_F - 298.67\right) + 4.297e^{-5}\log\left(P_{H_2}\sqrt{P_{O_2}}\right)T_F, \tag{6}$$

$$P_{H_2} = \frac{1}{2}RH_{Ap} * P^{sat}_{H_2O}\left(\frac{1}{\left(RH_{Ap} * P^{sat}_{H_2O}/P_{Ap}\right)\exp\left(1.59 * \left(I_c/A\right)/T_{Fo}\right)}\right), \tag{7}$$

$$P_{O_2} = \frac{1}{2}RH_{Cp} * P^{sat}_{H_2O}\left(\frac{1}{\left(RH_{CE} * P^{sat}_{H_2O}/P_{CE}\right)\exp\left(4.10\left(I_s/A\right)/1.299 * T_F\right)}\right), \tag{8}$$

$$V_{AL} = z_1 + z_2T_F + \left(z_3 + z_4\right)T_F * \log\left(C_{O_2} + I_S\right). \tag{9}$$

4. Design and Performance Study of Various MPPT Controllers

From the literature study, all of the renewable energy systems' power supply is nonlinear. So, the direct power supply from the renewable energy systems to the local consumers is not possible. So, the power electronics devices are used in the renewable power supply systems for maintaining the constant load to the electric vehicle systems [64]. However, the functioning point of all renewable power systems is not constant. So, there are various categories of MPPT methodologies that are applied to the renewable power supply network to identify the operating point of the fuel stack. From the literature review, the MPPT controllers are differentiated as artificial intelligence, machine learning, nature-inspired, soft computing, and fuzzy logic controllers. In [65], the authors discussed the fundamental power point tracking methods that are suitable for constant functioning temperature conditions of the fuel stack. So, in this work, soft computing methodologies are selected for optimizing the fluctuations across the fuel stack MPP position. In this work, the studied MPPT methodologies are Multilayer Neural Network Controller (MLNNC), Genetic Controller optimized Artificial Neural Controller (GCOANC), Adjustable Step Change of Fuzzy Controller with (ASCFC), Continuous Step Variation of Hill Climb-dependent FC (CSVHCFC), and Grey Wolf Algorithm-based FC (GWAFC).

4.1. Multilayer Neural Network Power Point Tracking Controller. From the previously existing power point tracking controllers, the conventional methodologies are selected where the accuracy of MPP finding is not needed. The conventional methodologies are suitable for traffic controlling control systems and constant operating

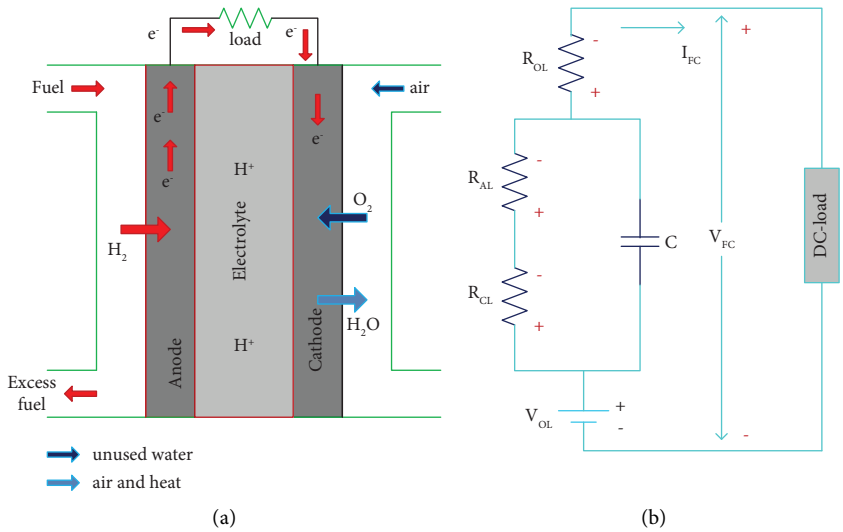

Figure 3: Polymer membrane fuel stack. (a) Structure. (b) Functioning circuit.

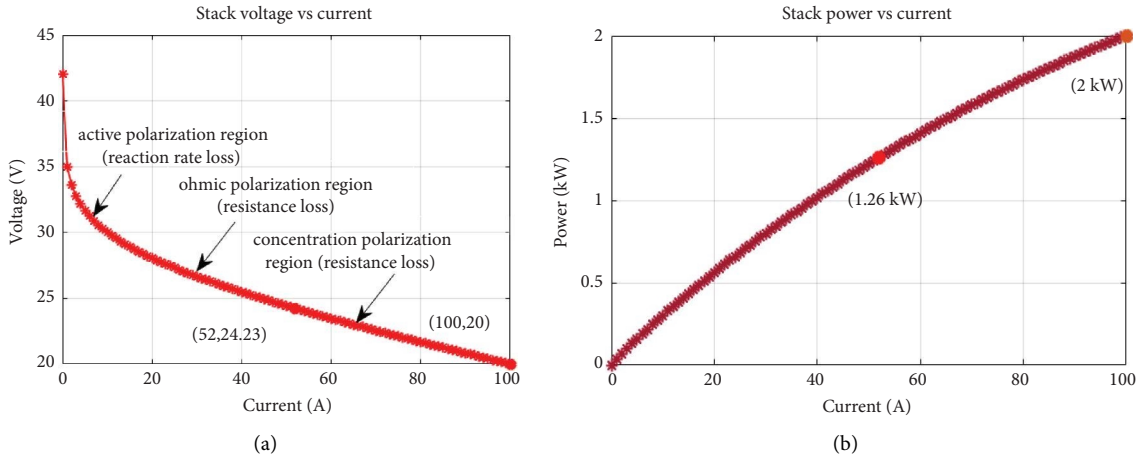

Figure 4: (a) V-I curve of the utilized fuel stack and (b) P-I curve of the PEMFSM.

Table 3: Design variables of selected fuel stack network.

Parameters	Values
Selected rated power of the overall network	6.0 kW
The selected potential across two electrodes (V_{MPP})	45.002 V
Collected current between the two electrodes (I_{MPP})	133.4 A
Collected voltage of the fuel stack at open circuit (V_{OC})	65.89 V
The generated oxygen pressure inside the fuel stack	1.2 bar
Utilized hydrogen pressure in the fuel stack	1.72 bar
Overall utilized fuel cells in the entire stack (N)	66.0
Basic air flow in the overall fuel stack (I_{pm})	533.19
Rated value of the gas constant (R)	87.229 ($J \cdot mol^{-1} \cdot K^{-1}$)
Faraday constant of the fuel stack (F)	95,118.551 ($C \cdot mol^{-1}$)
Available oxygen decomposition rate	20.22%
Available hydrogen decomposition rate	99.66%
Overall reaction rate of the hydrogen decomposition	98.889%
Overall reaction rate of the oxygen decomposition	59.99%
Standard temperature constant of the fuel stack	335 Kelvin

temperature conditions of the solid oxide fuel stacks. In [66], the authors proposed the multiple layers involved in neural networks for operating the polymer membrane fuel stack network under various environmental operating temperature conditions. Here, all the neural controllers were developed based on the human brain functioning conditions. The multilayer neural network MPPT controller utilized structure is shown in Figure 5. Based on the multilayer structure, the selected input neurons in the first layer are two which are fuel stack supply current ($M_1^{(1)} = I_{\mathrm{FC}}$) and fuel stack supply voltage ($M_2^{(1)} = V_{\mathrm{FC}}$). The middle layer collects the signals from the source layer, and the middle layer neurons are 629. Due to this large number of neurons and their corresponding layers, the multilayer neural network takes more data training time, and it requires high convergence time [67]. Here, the weights of the neurons are adjusted by utilizing the backpropagation algorithm which is given in (10) and (11) . Here, the terms $f(n)$, b, k, and L are the activation function, the total number of hidden layer nodes, the hidden layer output, and the output node. Finally, the variable "v" defines the overall neurons in between the input and output layers.

$$n_v^{(2)}(b) = \sum_{n=1}^{2} w_{\mathrm{vn}}^{(2)} * m_v^1;\ v = 1,\ 2,\ 3.4\cdots, 5\cdots b, \tag{10}$$

$$k_v^{(2)}(b) = T\left(N_n^{(2)}(b)\right), \tag{11}$$

$$L^3(v) = \sum_{v=1}^{5} w_v^{(3)} * k_v^{(2)}, \tag{12}$$

$$w_{\mathrm{vn}}^{(2)} = w_{\mathrm{vn}}^{(2)} + \Delta w_{\mathrm{vn}}, \tag{13}$$

$$w_f^{(3)} = w_{f3}^{(3)} + \Delta w_f, \tag{14}$$

$$\begin{aligned} \Delta w_{\mathrm{vn}} &= i * \frac{\partial e}{\partial w_{\mathrm{vn}}^{(2)}}, \\ \Delta w_v &= i * \frac{\partial e}{\partial w_v^{(3)}}. \end{aligned} \tag{15}$$

After weight updating of all the neurons, there is an error existing in the output layer which is given in (16). From (16), the terms V_{required} and V are the required peak voltage and available fuel stack voltage.

$$\mathrm{error} = \frac{1}{2}\left(V_{\mathrm{required}} - V^{(3)}\right)^2. \tag{16}$$

4.2. Genetic Controller Optimized Artificial Neural Network Controller. The genetic optimization methodology is used in [68] to identify the functioning point of the solar and fuel stack system. This algorithm does not require any derivate information. The merits of this algorithm are more exploration of search space, good flexibility, more adaptability, good parallel processing information, and global optimization. However, this algorithm has many disadvantages which are more computational complexity, high difficulty in tuning parameters, more dependence on randomness, risk of premature convergence, and limited understanding of results. So, the genetic algorithm is combined with the proportional and integral block to improve the steady-state response of the system and maintain the transient stability of the overall system. In [69], the genetic controller is combined with the artificial neural network for tracking the MPP of the hybrid wind/PV/FS power generation system with high efficiency. Here, initially, the neural network collects the signals from the fuel stack and solar networks which are sunlight intensity, fuel stack power, solar power, and functioning temperature of all the sources for moving the functioning point of the overall system from the initial stage to the required MPP location. Once, the functioning point of the hybrid network stabilizes with the actual MPP point, then the hill climb starts working to generate the highly accurate nonlinear power characteristics of the system [70]. The overall training samples considered in this neural network are 689. The operation of a genetic algorithm-dependent neural controller is given in Figure 6. From Figure 6, the generated error signal from the neural controller is monitored by applying the proportional controller. Here, the continuous changes in fuel stack temperature (T_{FC}), water membrane (T_M), fuel stack current (I_F), and voltage (V_F) are selected for generating the duty signal to the DC-DC converter. The time constant of the integral controller is $\mathrm{T_{ic}}$, and finally, the constraints of the proportional and integral controllers are S_P and S_i.

$$\mathrm{error}(n) = V_{\mathrm{MPP}}(n) - V_F(n), \tag{17}$$

$$S(n) = S_p \mathrm{error}(n) + \frac{S_i}{T_{\mathrm{ic}}} \int \mathrm{error}(n) * \mathrm{d}n, \tag{18}$$

$$P_S^b = f\left(\mathrm{net}_s\right) = f\left[\sum_{s=1}^{p} W_{\mathrm{sb}} * Z_a + W\right], \tag{19}$$

$$\mathrm{error} = \frac{1}{2}\sum_{s=1}^{R}\left(D_s - Q_s^b\right)^2, \tag{20}$$

$$W_{\mathrm{sb}}(n+1) = W_{\mathrm{sb}}(n) + \mu * \Psi_s * T_i, \tag{21}$$

$$W_{\mathrm{ks}}(n+1) = W_{\mathrm{ks}}(n) + \mu * \Psi_s * T_i. \tag{22}$$

From (19) and (20), the parameters "n", S, W, P, b, a, h, Q, μ, and ψ are the number of neurons, number of iterations, weight of neurons, middle layer constants, output layer constants, time constant of the proportional controller, and weight updating constants. Also, the parameters T_{ic}, U, and D are input variable, hidden layer, and duty signal of the DC-DC converter.

4.3. Adjustable Step Change of Fuzzy Controller with Incremental Conductance. Conventional neural networks take more time to achieve the optimal nonlinear solution of the fuel stack network because it takes more convergence time,

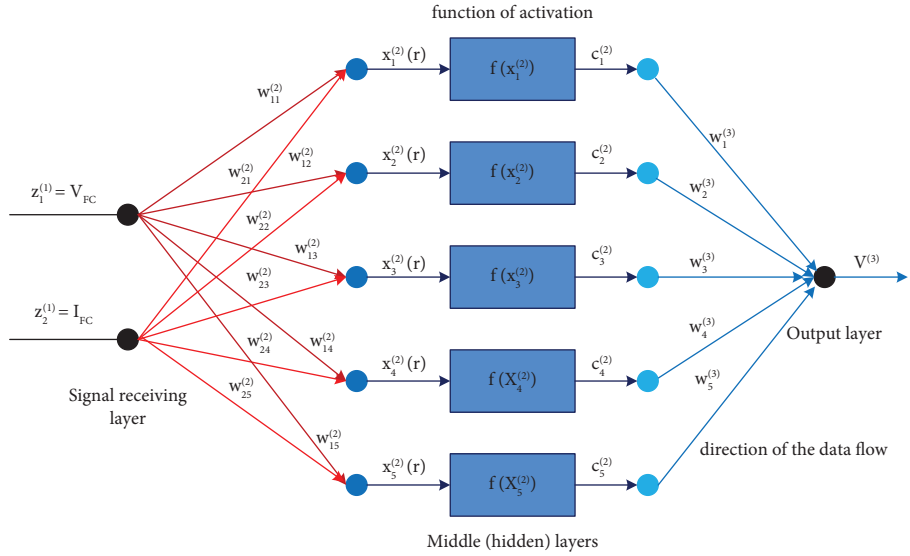

Figure 5: Working structure of multilayer neural network MPPT controller.

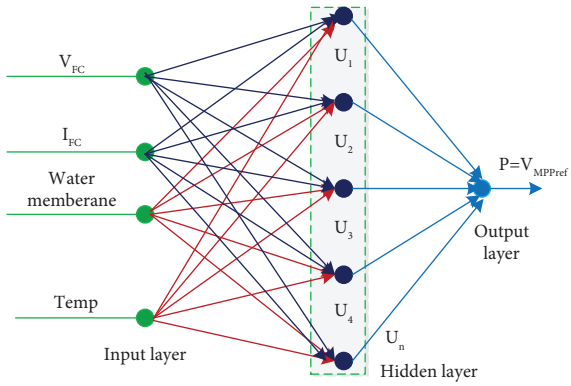

Figure 6: Genetic algorithm-related artificial intelligence-based MPPT controller.

high training data are needed when the neural network involves multiple layers in the structure, and it is less suitable for continuous changes of the environmental conditions of the fuel stack network [71]. So, the artificial neural network limitations are overcome by using the fuzzy logic controller. Fuzzy logic is one type of approach which is used to process the variable towards the true value. Most of the fuzzy controllers are used for solving highly complex nonlinear problems. The features of fuzzy systems are easy to implement, highly robust, more flexible, good interpretability, and easy to understand. However, the fuzzy logic MPPT controller may not be accurate in the MPP position. In addition, it cannot recognize the neural network and machine learning patterns. Also, it required a highly knowledgeable person to implement the fuzzy logic controller, was very difficult in tuning, less accurate in MPP tracking, and had high computational complexity [72]. So, the fuzzy logic is combined with the incremental conductance method for reducing the tracking time of the fuel stack MPP. Here, initially, the fuzzy controller methodology is used for adjusting the step value of the IC controller for optimizing the oscillations across the fuel stack MPP position. The functioning diagram of this MPPT controller is given in Figure 7. From Figure 7, the continuous variation of fuel stack current (I_{FC}) and voltage (V_{FC}) are collected and the resultant error signal is given to the incremental conductance controller. H_{vold} and H_{vnew} are the previously stored fuel stack V-I curve slope and present available fuel stack slope. The terms D, ΔV, and ΔP are the converter duty signal, change of fuel stack voltage, and change of power.

$$D(v) = D(v-1) + H_{Vnew}\text{sig}\left(\frac{\Delta I}{\Delta V} + \frac{I}{V}\right), \tag{23}$$

$$\begin{aligned} H_{Vnew} &= \text{step}\frac{\Delta P}{\Delta V}; \\ H_{vold} &= \frac{\Delta P}{\Delta V} = \frac{P(b) - P(b-1)}{V(b) - V(b-1)}, \end{aligned} \tag{24}$$

$$D(v) = D(v-1) - H_{Vnew}\left(\frac{\Delta I}{\Delta V} + \frac{I}{V}\right). \tag{25}$$

4.4. Fuzzy Logic Controller-Dependent Hill Climb MPPT Controller. There are various conventional controllers available in the literature, which are Perturb & Observe and incremental conductance controllers. However, these controllers are not useful for the rapid changes in the functioning temperature conditions of the fuel stack. So, the researchers referred to the hill climb methodology in [73] for the hybrid wind/fuel stack network power supply system to meet the peak load demand of the local consumers. However, the implementation cost of the hill climb controller is very high when equated to the other controller. So, the fuzzy logic is combined with the hill climb controller to extract the peak power from the renewable energy system. Here, the fuzzy concept is applied to fix the step size value of the hill climb controller [74]. Here, the fuzzy logic block captures

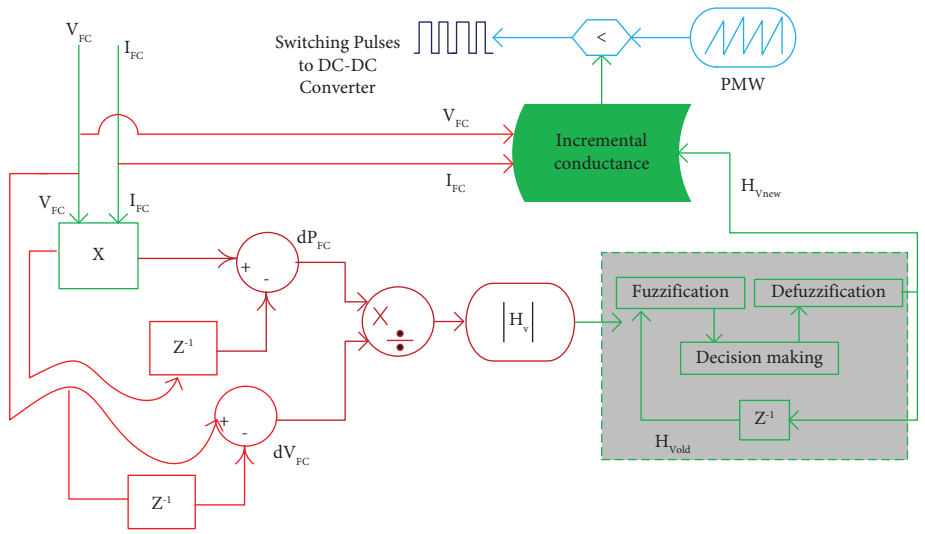

Figure 7: Block diagram of the fuzzy controller-based incremental conductance MPPT controller.

the overall data of the V-I curve of the fuel stack network. After collecting the overall data, the fuzzy logic identifies the local operating point of the fuel stack network. The variation of power (δP), variation of voltage (δV), and variation of current (δI) are utilized for identifying the duty cycle of the power converter. The past converter duty cycle $D(m-1)$, past power $P(m-1)$, and past current $I(m-1)$ are compared with the present variables $D(m)$, $P(m)$, and $I(m)$.

$$\delta P = P(m) - P(m-1), \tag{26}$$

$$\delta I = I(m) - I(m-1), \tag{27}$$

$$\delta D = D(m) - D(m-1). \tag{28}$$

4.5. Optimization of Fuzzy Logic Controller by Using Modified Grey Wolf Optimizer. Most of the neural network-based power point tracking controllers required high training data of the polymer membrane fuel stack system [75]. Also, it required well-experienced person to select the number of layers in the neural network structure. The drawbacks of neural controllers are overcome by utilizing fuzzy systems. In the fuzzy system, the selection of a membership function is a very difficult task and its functioning efficiency depends on the accuracy of membership function selection. In the literature, there are various optimization technologies that are applied to optimize the membership function values. Here, in this article, the modified grey wolf methodology is used to improve the functioning efficiency of the fuzzy controller. The pseudocode of the modified grey wolf controller is shown in Figure 8. From Figure 8, the selected fuel stack variables for finding the duty signal value of the DC-DC converter are fuel stack current, fuel stack power, and fuel stack voltage. In this grey wolf method, the collected data from the fuel stack are assigned to the various wolves.

Here, all the wolves start searching for the optimized duty value by interchanging their information towards the required objective identification. In the first iteration, the wolves move in different directions with different velocities. After reaching certain iterations, the wolves move in one direction to find the optimal solution for the nonlinear problem of the fuel stack network. Finally, the grey wolf controller tries to make the system stabilize at any one of the local MPP positions of the fuel stack network. After that, the grey wolf controller gives the information to the fuzzy block as shown in Figure 9. From Figure 9, the fuzzy logic system consists of three major blocks which are fuzzification, inference network, and defuzzification network. In the fuzzification system, the input supply variables are transferred into fuzzy sets. The inference network collects the fuzzy sets for generating the required output of the fuel stack. Finally, the defuzzification methodology is used for transferring the fuzzy outputs into crisp solutions. The fuzzy logic starts identifying the global functioning point of the fuel stack. Here, (29) is used to move the functioning point of the fuel stack from the origin position of the V-I curve to the global MPP place. Sometimes, the working point of the fuel stack is on the right-hand side of the V-I curve of the fuel stack and then (30) is used to move the functioning point of the fuel stack towards the actual MPP place. From (29) and (30), the variables ψ, $\text{Power}_{\text{present}}$, and $\text{Power}_{\text{previous}}$ are the error stabilizing factor and fuel stack powers.

$P_{present}$ is =0,
Apply do while operation (e<= overall iterations completed)
Find out the required agents grey wolf method D_e (e=1, 2… z); D_e will be 0.1 to 0.9
Find out the constraints R, T, and L; R and W are suitable coefficients
Evaluate the suitable fitness value of each agent P_e(e=1,2,3, 4,5, 6, …z)
D_α; Converter duty value of the local best agent.
D_β: Second grey wolf assigned power converter duty value.
D_δ ; Third grey wolf assigned power converter duty value.
$P_{present}$ is equal to P (D_α)
Condition of Do while ($P_{present}$-$P_{previous}$) <ψ_1); here, ψ is error value
Continuous variation of wolf position and velocity
Upgrade the R, T, and L values for the wolf
Determine the fitness parameters values P_e (e=1,2,3,4,5, 6.…z)
Grey wolf parameters updating D_α, D_β, plus D_δ
Vary the power converter duty values D, D_1, D_2, and D_3; Here "D" defines the converter operating duty value.
$P_{present}$ is equal to $P_{previous}$ then $P_{present}$ is equal to P(D_α)
C=c+δc
Ends Do
Cc is equal to 0
Starts Do while operation ($P_{present}$-$P_{previous}$) <ψ_2)
Utilize the fuzzy concept for determining the fuel stack power and voltage
Cc=cc+ δ_{cc}
End do
End do

Figure 8: Working pseudocode of the proposed power point tracking controller.

$$\left|\text{Power}_{present} - \text{Power}_{previous}\right| \leq \psi_1, \tag{29}$$

$$\left|\text{Power}_{present} - \text{Power}_{previous}\right| \geq \psi_2. \tag{30}$$

5. Development of Single Switch Universal Supply Voltage Boost Converter

From the literature study, the isolated power DC-DC converters are not applied for fuel stack running electric vehicle applications because of its disadvantages such as more implementation cost, high space requirement for installation, less efficiency for electric vehicle systems, and difficulty in developing the switching circuit [76]. So, transformerless power converter networks are used in automotive systems for the effective running of hydrogen-dependent vehicles. Here, in this work, the unique power Metal Oxide Semiconductor Field Effect Transistor (MOSFET) is used for enhancing the fuel stack supply voltage from one level to another level. The features of MOSFET are high voltage withstanding ability, more switching speed, less power consumption, very little power dissipation, high input impedance, more power control capability, less driver circuit implementation complexity, and high temperature withstanding ability. The utilized diodes in this proposed converter circuit are D_q, D_w, D_e, and D_t. Similarly, the selected capacitors in the wide output voltage range DC-DC converter are C_l, C_j, C_k, C_h, and C_g. The available inductors and resistors in the converter are L_q, L_w, and R_n. When the converter starts working, the currents flowing through capacitors and inductors are I_{Cl}, I_{Cj}, I_{Ck}, I_{Ch}, I_{Cg}, I_{Lq}, and I_{Lw} and the voltages appearing across those elements are V_{Cl}, V_{Cj}, V_{Ck}, V_{Ch}, V_{Cg}, V_{Lq}, and V_{Lw}. Finally, the voltages appearing across the switches and diodes are V_S, V_{Dq}, V_{Dw}, V_{De}, and V_{Dt}. The detailed working structure of the converter is shown in Figures 10(a), 10(b), and 10(c). The switching states of the converter are given in Table 4.

5.1. Working Stage of Converter (DCCM and CCM): I. In this stage, the converter works in both the stages of operation which are Discontinuous Conduction Mode (DCCM) and Continuous Conduction Mode (CCM). These modes of operation purely depend on the input inductor selection value. Suppose, the selected inductor L_q value is more than the converter works in the continuous power supply stage. Otherwise, the utilized power converter works in discontinuous power supply mode. Here, the source is a polymer membrane fuel module for automotive applications. So, the selected input supply inductor value should be very high to work in the continuous power supply mode of operation of

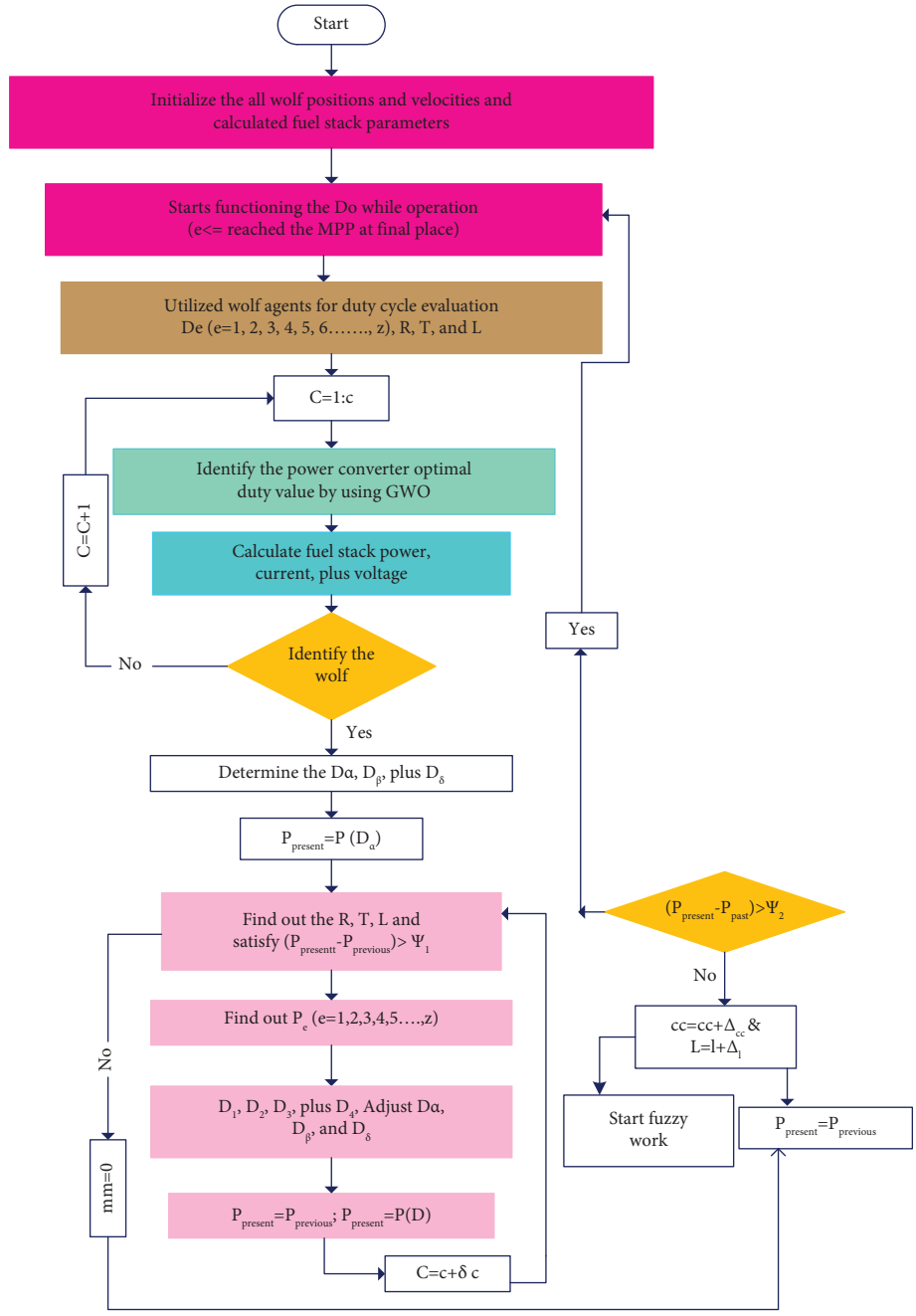

FIGURE 9: Overall working structure of the fuzzy membership functions optimized grey wolf MPPT controller.

the converter. In this stage, the switch (S) starts working in forward bias condition and then the inductors start absorbing the source currents and voltages which are identified as $I_{Lq-chrg}, I_{Lw-chrg}, V_{Lq-chrg}$, and $V_{Lw-chrg}$. After a certain time duration, the inductors start delivering the currents and voltages which are defined as $I_{Lq-dicg}, I_{Lw-dicg}$, $V_{Lq-dicg}$, and $V_{Lw-dicg}$. Similarly, the capacitors' $(C_l, C_k, C_j, C_h, \text{and } C_k)$ stored currents and voltages are $I_{Cl-chrg}, I_{Ck-chrg}, I_{Cj-chrg}, I_{Ch-chrg}, I_{Cg-chrg}, V_{Cl-chrg}$, $V_{Ck-chrg}$. $V_{Cj-chrg}, V_{Ch-chrg}$, and $V_{Cg-chrg}$. Finally, the capacitors' discharging parameters are represented as $I_{Cl-dicg}, I_{Ck-dicg}, I_{Cj-dicg}, I_{Ch-dicg}, I_{Cg-dicg}, V_{Cl-dicg}$, $V_{Ck-dicg}$. $V_{Cj-dicg}, V_{Ch-dicg}$, and $V_{Cg-dicg}$. The converter inductor charging voltages are given in Figures 11(a) and 11(b). From Figure 11(a), the capacitor voltages and inductor currents are derived in (31) and (32).

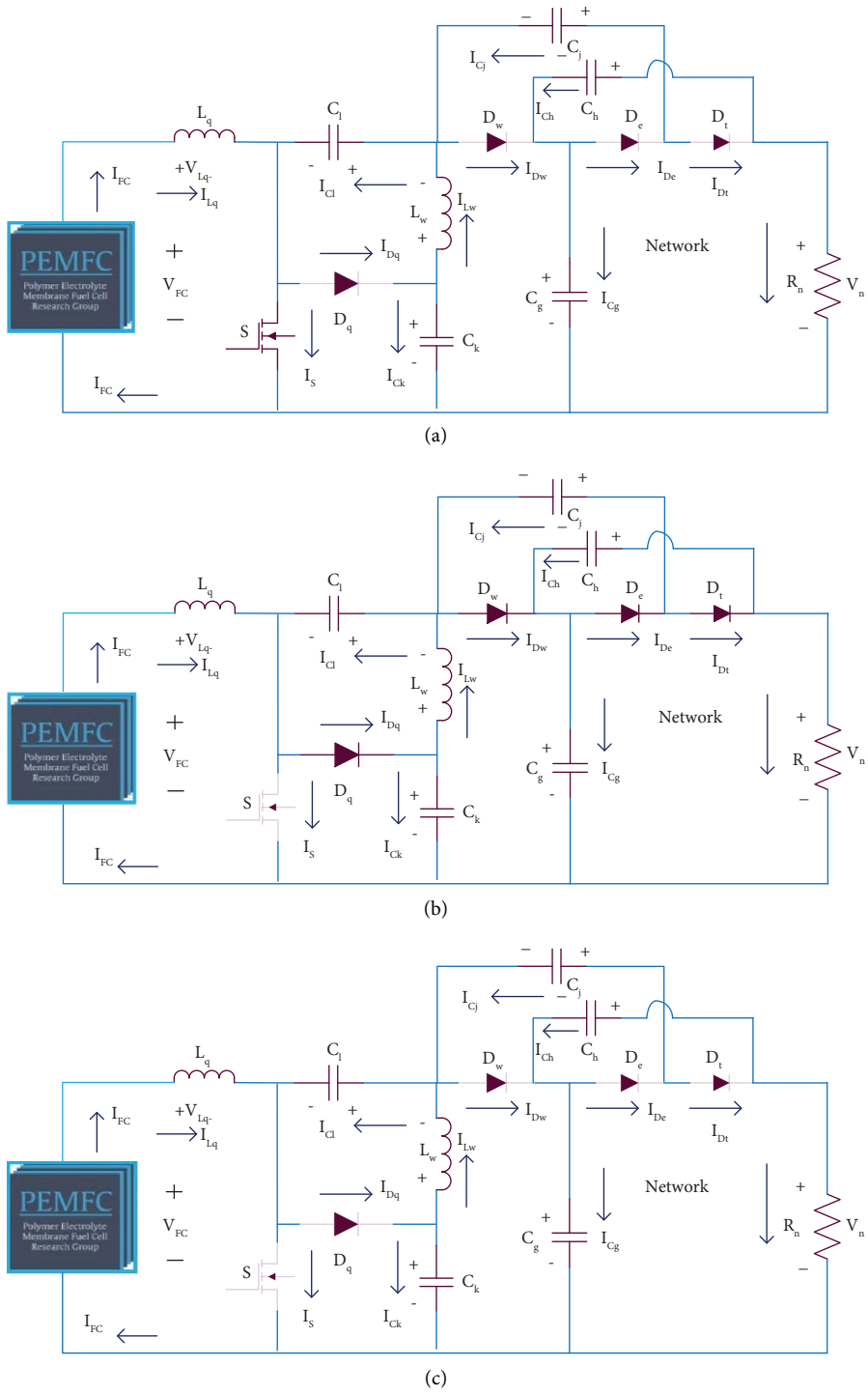

Figure 10: (a) Switch ON condition, (b) switch blocking state, and (c) both switch and diodes are in a blocking state.

Table 4: Functioning stages of wide input voltage proposed DC-DC converter.

Elements	DCCM and CCM at first stage	DCCM and CCM at second stage	DCCM at third stage
S	ON	OFF	OFF
D_q	OFF	ON	OFF
D_w	OFF	ON	OFF
D_e	OFF	ON	OFF
D_t	OFF	ON	OFF

$$\begin{cases} V_{\mathrm{Lq}} = V_{\mathrm{FC}}, \\ V_{\mathrm{Lw}} = V_{\mathrm{Ck\_dicg}} - V_{\mathrm{Cl\_chrg}}, \end{cases} \tag{31}$$

$$\begin{cases} I_{\mathrm{Cj\_chrg}} = I_S - I_{\mathrm{Lq}}, \\ I_{\mathrm{Ch\_chrg}} - I_{\mathrm{Cg\_chrg}} = I_{Lw} = -I_{\mathrm{Ck\_dicg}}, \\ I_{\mathrm{Ch\_dicg}} = I_{\mathrm{Cj\_chrg}} + I_{\mathrm{Cg\_dicg}} = -I_n, \end{cases} \tag{32}$$

$$\begin{cases} V_{\mathrm{Lq}} = V_{\mathrm{FC}} - V_{\mathrm{Ck\_chrg}}, \\ V_{\mathrm{Lw}} = V_{\mathrm{Ck\_chrg}} - V_{\mathrm{Cg\_chrg}}, \end{cases} \tag{33}$$

$$\begin{cases} I_{\mathrm{Cq\_dicg}} = I_{\mathrm{Dq}} - I_{\mathrm{Lq}}, \\ I_{\mathrm{Cj\_dicg}} = I_{\mathrm{Dw}} + I_{\mathrm{Cq\_dicg}} - I_{\mathrm{Lw}}, \\ I_{\mathrm{Ck\_chrg}} = I_{\mathrm{Lw}} - I_{\mathrm{Dq}}, \\ I_{\mathrm{Ch\_chrg}} = I_{\mathrm{Cg\_chrg}} - I_{\mathrm{Dw}}, \end{cases} \tag{34}$$

$$V_{\mathrm{Lq\_Minimum}} = V_{\mathrm{Lw\_Minimum}} = 0, \tag{35}$$

$$I_{\mathrm{Lq\_Minimum}} + I_{\mathrm{Lw\_Minimum}} = 0. \tag{36}$$

5.2. Working Stage of Converter (DCCM and CCM): II and III. In the second mode of converter operation, the available voltage across the MOSFET is reduced and the switch starts moving from the amplifying stage to the blocking stage. Here, the capacitors C_l and C_w give the energy to the load side capacitors $C_j, C_h,$ and C_g. From Figure 11(b), the switch-off voltage in the converter flows towards the diodes to make the diodes run in the active region condition. From Figure 12(c), all the switches and diodes are going into the discontinuous functioning stage. As a result, the polymer membrane fuel stack network supplies fluctuated power which is desirable for the four-wheeler electric vehicle network. Here, the switching voltages and currents are completely in a zero-level state. Under steady-state operation of a single switch more power conversion ratio of the DC-DC converter, the available voltage at the load side is derived in (38). The converter operated duty is defined as D and the time duration of the converter voltage is represented as T_S. Under the discontinuous functioning stage of the converter, the time duration of the converter current is T_x. The selected load parameter in the converter is the resistor (R_n) and its corresponding current and voltage are identified as V_n and I_n.

$$V_{\mathrm{Cq}} = \frac{D}{(1-D)} * V_{\mathrm{FC}}, \tag{37}$$

$$V_{\mathrm{Cj}} = V_{\mathrm{Ck}} = V_{\mathrm{Ch}} = \frac{1}{(1-D)} * V_{\mathrm{FC}}, \tag{38}$$

$$V_{\mathrm{Cg}} = \frac{1+D}{(1-D)} * V_{\mathrm{FC}}, \tag{39}$$

$$V_n = \frac{2+D}{(1-D)} * V_{\mathrm{FC}}, \tag{40}$$

$$\mathrm{Gain}_{\mathrm{CCM}} = \frac{V_n}{V_{\mathrm{FC}}} = \frac{2+\mathrm{D}}{(1-\mathrm{D})}, \tag{41}$$

$$\begin{cases} V_S = V_D = \dfrac{1}{(1-D)} * V_{\mathrm{FC}}, \\ V_D = V_{\mathrm{Dq}} = V_{\mathrm{Dw}} = V_{\mathrm{De}} = V_{\mathrm{Dt}}, \end{cases} \tag{42}$$

$$V_S = V_D = \frac{2+\mathrm{Gain}_{\mathrm{CCM}}}{3\mathrm{Gain}_{\mathrm{CCM}}} * V_{n,} \tag{43}$$

$$I_{\mathrm{Lw}} = I_{\mathrm{Lq}} = I_n, \tag{44}$$

$$I_{\mathrm{Lw}} = \frac{2+\mathrm{D}}{1-\mathrm{D}} * I_n = \mathrm{Gain}_{\mathrm{CCM}} * I_n. \tag{45}$$

From the literature study, the power converter study has been done in terms of their working efficiency. Here, in this article, investigation of various categories of power electronics converters has been done in terms of voltage gain availability, total number of semiconductors devices applied for designing the converter, voltage appeared across the switch, type of current flow in the converter circuit, and necessity of ground required for the power converter. In [54], the authors utilized the general nonisolated converter structure for the microgrid power supply system to improve the voltage stability of the fuel stack network. The advantages of this converter are simple in structure, good reliability, high robustness, and more adaptability. However, this converter needs a high operating duty cycle for high voltage-rating electric vehicle applications. As a result, the entire fuel stack power supply network conduction losses are increased extensively. So, the wide output voltage gain, universal supply voltage power converter circuit is utilized in this work for continuous power supply to the automotive system. The voltage gain and current stress of the proposed converter are given in Table 5.

6. Analysis of Simulation Results

The proposed system involves the polymer membrane fuel stack and power point tracking controller along with the high voltage gain DC-DC converter. As of now, the polymer membrane-based fuel stack modules are used for electric vehicle systems because of their features such as high temperature withstanding ability, less atmospheric pollution, easy functioning, less maintenance required, more lifetime, and easy installation. However, the polymer membrane fuel system generates nonlinear power characteristics. So, the identification of the functioning point of the fuel stack is quite difficult work. In addition, the available source voltage is very low which is not acceptable for industrial as well as local consumer applications. So, the hybrid power point tracking controller is introduced in this work for catching the exact position of the polymer membrane fuel stack network. The merits of this MPPT controller are its ability in identifying MPP location quickly, fewer iteration requirement for identifying the local MPP position, better

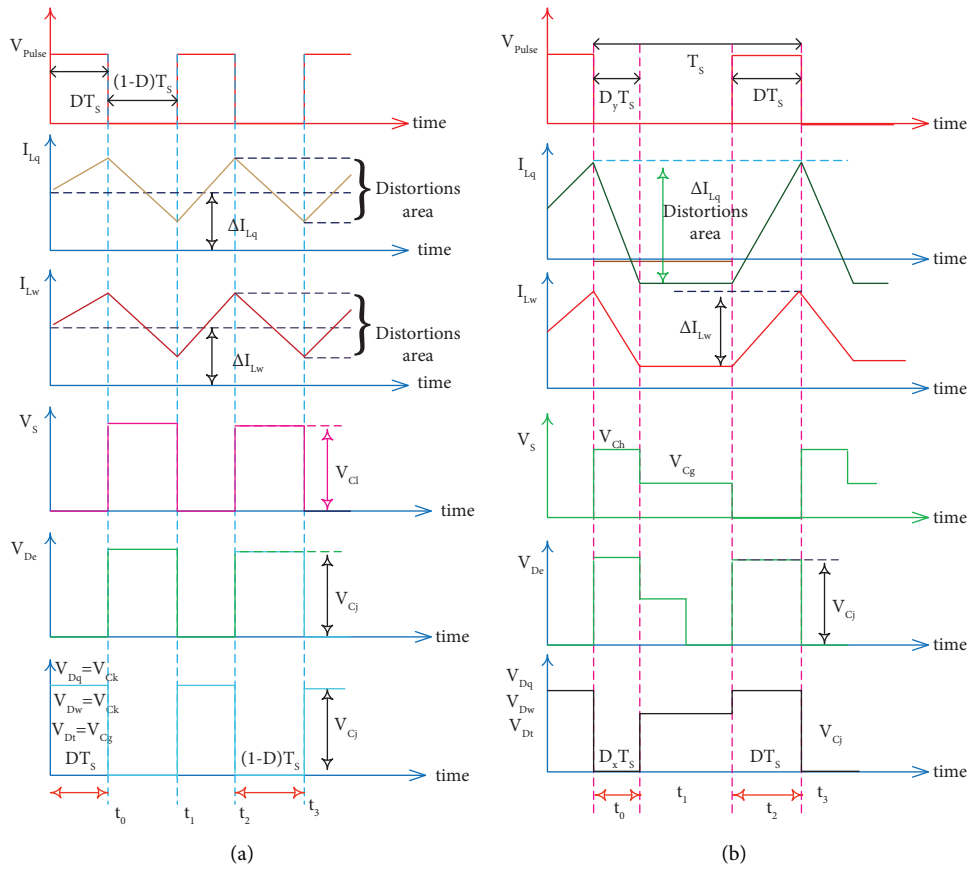

Figure 11: (a) Working of the converter under continuous power supply mode and (b) fluctuated power supply mode.

dynamic response of the system, and being most suitable for rapid changes of operating temperature conditions of the fuel stack system. Here, the fuel stack current flow is optimized by utilizing the single switch power DC-DC converter.

6.1. Analysis of Overall Proposed System at Static Temperature (325 K). The selected supply side capacitors (C_l, C_j, C_k, C_h, and C_g) for the design of the power converter are 32.5 μF, 37.99 μF, 58.55 μF, 58.55 μF, and 45.37 μF, respectively. Similarly, the utilized inductor (L_q and L_w) values are 260 μH, and 280 μH, respectively. The source side inductor L_q tries to suppress the distortions of fuel stack voltage and power. The capacitor C_l helps stabilize the fuel stack voltage and removes the sudden various source voltages to protect the switch "*S*." Here, the proposed system is studied at uniform working temperature conditions of the fuel stack which is selected as 325 K. The converter modeling has been done by utilizing the MOSFET switch and the selected load resistor value is equal to 85 Ω. The utilized parameters for tracking the fuel stack network MPP are fuel stack power, current, and voltage. These variables help linearize the overall system and optimize the duty cycle of the power DC-DC converter. The available fuel stack supply current and fuel stack voltages are given in Figures 12(a) and 12(b). The converter's functioning duty signal and its related current, voltage, and powers are shown in Figures 12(c)–12(f) From Figures 12(a) and 12(b), the available current and voltage parameters of the fuel stack under static temperature conditions by applying the MLNNC, GCOANC, ASCFC, CSVHCFC, and GWAFC are 112.7 A, 39.84 V, 112.82 A, 40.53 V, 112.44 A, 40.76 V, 111.81 A, 42.13 V, 110.32 A, and 43.48 V, respectively. These high available currents and lower voltages of the fuel stacks are not useful for any local as well as industrial applications. So, the wide input supply voltage and less voltage stress-based DC-DC proposed converter is integrated with the source network and MPPT controller block for improving the load power, voltage, and current ratings. The achieved load current, voltage across the converter output, and load power by utilizing the MLNNC, GCOANC, ASCFC, CSVHCFC, and GWAFC MPPT controllers are 8.213 A, 527.32 V, 4330.87 W, 8.38 A, 528.72 V, 4430.67 W, 8.412 A, 530.33 V, 4461.13 W, 8.672 A, 534.8 V, 4637.78 W, 8.79 A, 535.99 V, and 4711.35 W, respectively. At static functioning temperature conditions of the fuel stack, the GWAFC-fed fuel stack supply voltage stabilizing time is 0.015 sec which is very

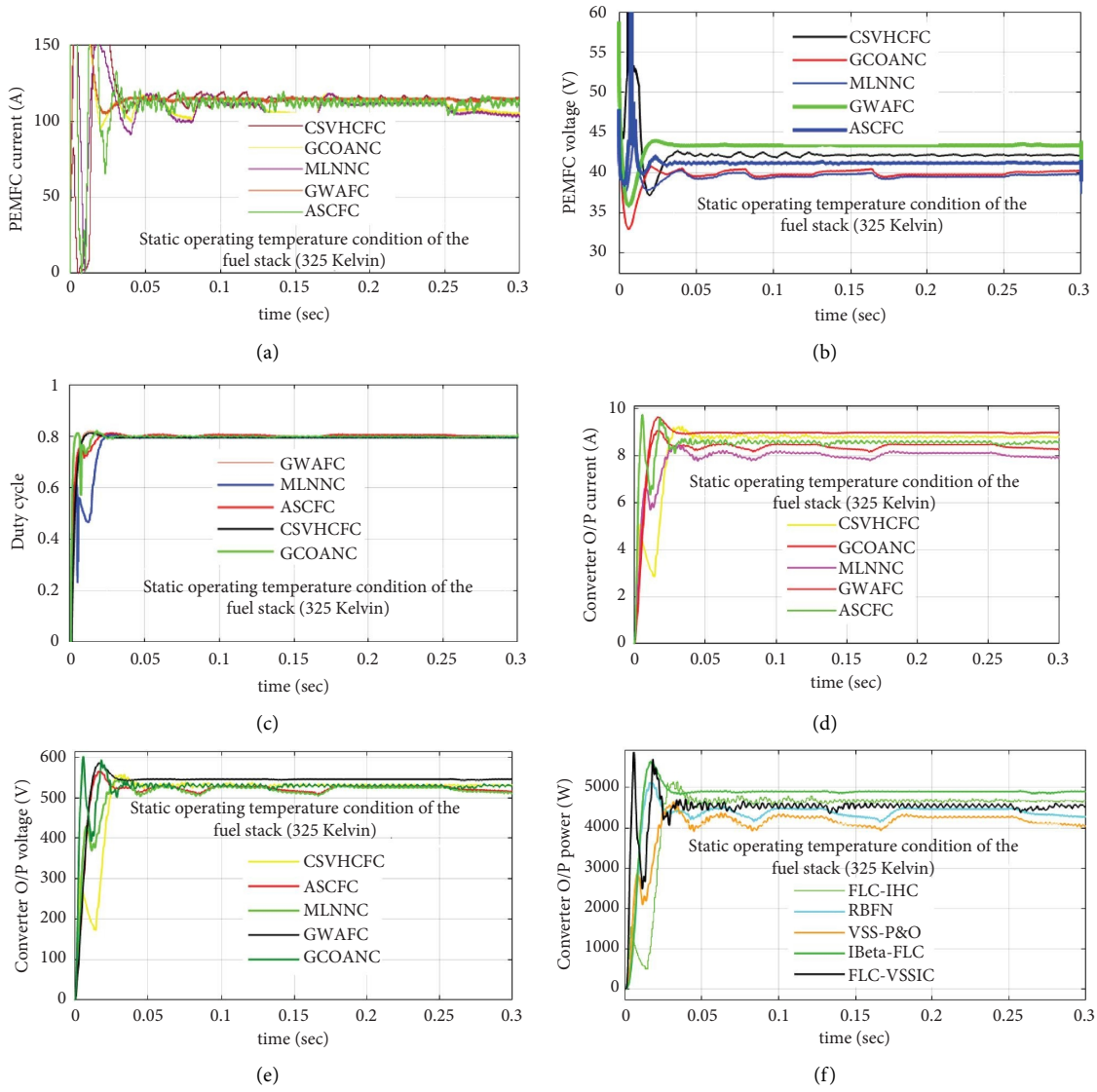

Figure 12: (a) Source current, (b) source voltage, (c) duty cycle, (d) load O/P current, (e) load O/P voltage, and (f) load O/P power at 325 Kelvin.

small when equated to the other power point tracking controllers. Also, the design and implementation cost is very moderate when compared to the CSVHCFC.

6.2. Analysis of Overall Proposed System at Dynamic Temperature (325 K, 305 K, and 345 K). Here, the overall system is studied at continuous variation of the functioning temperature of the fuel stack. At 305 K temperature, the extracted current values, voltage values, and power values of the fuel system by utilizing MLNNC, GCOANC, ASCFC, CSVHCFC, and GWAFC-based power point tracking controllers are 105.91 A, 39.66 V, 4200.52 W, 105.99 A, 40.87 V, 4332.15 W, 106.51 A, 40.85 V, 4351.97 W, 107.21 A, 40.63 V, 4356.07 W, 107.89 A, 39.90 V, and 4305.25 W, respectively. From Figures 13(a) and 13(b), the extracted peak current and voltage of the fuel stack are reduced when the functioning temperature of the source is reduced. So, the source power is directly proportional to the supply temperature of the fuel stack and its hydrogen decomposition. From Figure 13(c), the converter functioning duty cycle by utilizing the different adaptive MPPT controllers is approximately 0.79 to 0.811. The converter-optimized current rising and stabilizing times by introducing the GWAFC are 0.02 sec and 0.039 sec which are shown in Figure 13(d). Based on Figure 13(e), the available converter voltage is high at the supply temperature of 325 K and it suddenly falls at 305 K temperature. The fuel stack supply temperature is constant from 0 sec to 0.3 sec and steps down to 305 K from 0.3 sec to 0.6 sec. Finally, it is raised from 305 K to 345 K from 0.6 sec to 0.9 sec. At dynamic temperature conditions, the overall network load power fluctuations by integrating the various MPPT methodologies are shown in Figure 13(f). At 345 K, the entire load current, load voltage, and load powers by applying the MLNNC, GCOANC, ASCFC, CSVHCFC, and GWAFC-based MPPT blocks are 9.269 A,

Table 5: Analysis of various categories of power electronics converters for renewable energy systems.

Network	Gain conversion	Components needed	Ground needs	Passive components	Current flow	Switch strain	Diode strain
ZSBPC [77]	$1/D(1-D)$	Three switches, plus three diodes	Required	Two capacitors and two inductors	Distorted fashion	$(1/2)+\sqrt{(1/4)-(1/\text{Gain}_{\text{CCM}})}$	$3/2+\sqrt{(1/4)-(1/\text{Gain}_{\text{CCM}})}$
TILBC [78]	$(1+D)/(1-D)$	Four diodes and two switches	Not required	Three capacitors and two inductors	Constant fashion	$(1+\text{Gain}_{\text{CCM}})/(2*\text{Gain}_{\text{CCM}})$	$(1+\text{Gain}_{\text{CCM}})/(2*\text{Gain}_{\text{CCM}})$
QZPC [79]	$(1+2D)/(1-D)$	Three diodes and one switch	Required	Five capacitors and three inductors	Constant fashion	$(\text{Gain}_{\text{CCM}}+2)/(3*\text{Gain}_{\text{CCM}})$	$(\text{Gain}_{\text{CCM}}+2)/(3*\text{Gain}_{\text{CCM}})$
ITPBC [80]	$2/1-D$	Two diodes and two switches	Not required	Two capacitors and two inductors	Distorted fashion	0.5	0.5
HVDSBC [81]	$1/(1-D)(1+D)$	Three diodes and one switch	Required	Two capacitors and two inductors	Distorted fashion	1	1
BCPC [82]	$1/1-D$	One diode and one switch	Not required	One capacitor and one inductor	Constant fashion	1	1
Proposed converter	$(2+D)/(1-D)$	Four diodes and one switch	Required	Five capacitors and two inductors	Constant fashion	$(3+\text{Gain}_{\text{CCM}})/(4*\text{Gain}_{\text{CCM}})$	$(3+\text{Gain}_{\text{CCM}})/(4*\text{Gain}_{\text{CCM}})$

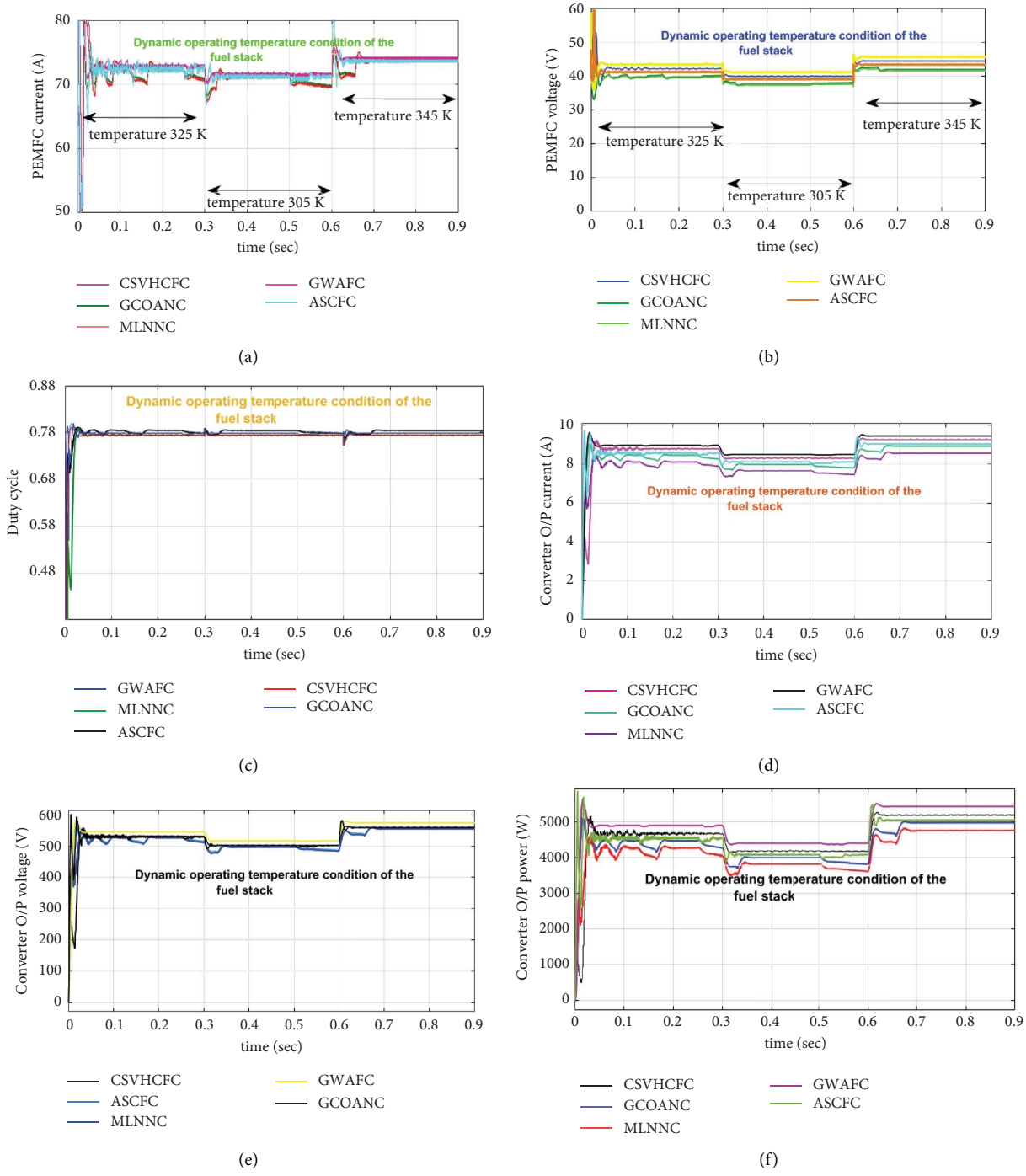

FIGURE 13: (a) Source current, (b) source voltage, (c) duty cycle, (d) load O/P current, (e) load O/P voltage, and (f) load O/P power at dynamic temperatures.

Table 6: Detailed analysis of various categories of power point tracking controllers at different operating temperature conditions of the fuel stack.

Type of MPPT	Fuel stack current (A)	Fuel stack voltage (V)	Fuel stack power (W)	Current of converter (A)	Voltage of converter (V)	Power of converter (W)	Working efficiency (%)	Settling time of voltage (sec)	Distortions of converter voltage	Complexity of MPPT controller
The functioning temperature of the polymer membrane fuel stack (325 K)										
MLNNC	112.7	39.84	4490.74	8.213	527.32	4330.87	96.44	0.039	High	Easy
GCOANC	112.82	40.53	4572.88	8.38	528.72	4430.67	96.89	0.028	High	Easy
ASCFC	112.44	40.76	4583.98	8.412	530.33	4461.13	97.32	0.022	High	Moderate
CSVHCFC	111.81	42.13	4711.27	8.672	534.8	4637.78	98.44	0.02	Moderate	Moderate
GWAFC	110.32	43.48	4797.22	8.79	535.99	4711.35	98.21	0.015	Low	Moderate
The functioning temperature of the polymer membrane fuel stack (305 K)										
MLNNC	105.91	39.66	4200.52	7.98	501.16	3999.32	95.21	0.027	High	Easy
GCOANC	105.99	40.87	4332.15	8.19	507.37	4155.4	95.92	0.052	High	Easy
ASCFC	106.51	40.85	4351.97	8.280	507.15	4199.22	96.49	0.045	High	Moderate
CSVHCFC	107.21	40.63	4356.07	8.287	509.46	4221.91	96.92	0.042	Moderate	Moderate
GWAFC	107.89	39.90	4305.25	8.291	509.61	4225.18	98.14	0.039	Low	Moderate
The functioning temperature of the polymer membrane fuel stack (345 K)										
MLNNC	194.10	27.99	5434.29	9.269	571.10	5293.55	97.41	0.031	High	Easy
GCOANC	198.02	27.28	5403.95	9.27	571.35	5296.42	98.01	0.025	High	Easy
ASCFC	198.20	27.07	5360.47	9.281	570.76	5297.22	98.82	0.021	High	Moderate
CSVHCFC	120.00	44.66	5360.28	9.30	569.86	5299.71	98.87	0.014	Moderate	Moderate
GWAFC	120.11	45.28	5438.95	9.312	577.77	5380.21	98.92	0.0172	Low	Moderate

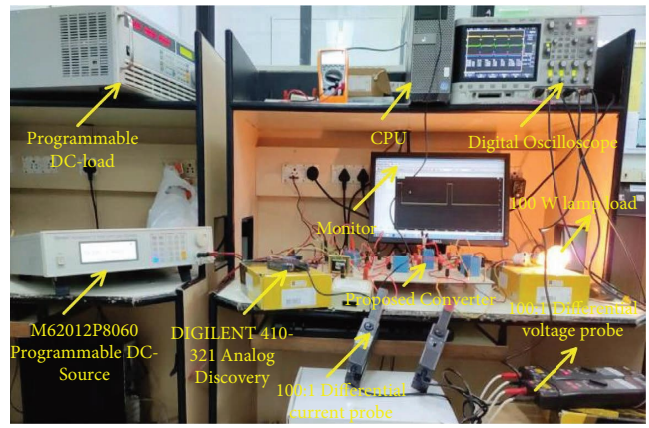

Figure 14: Testing of the proposed single switch power converter by using programming DC source.

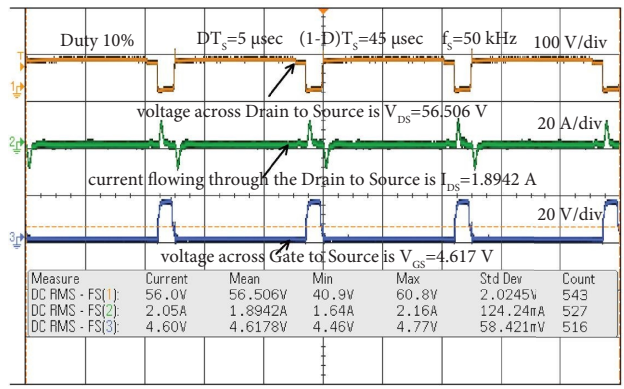

Figure 15: Evaluated converter switching voltages and currents at 10% duty value.

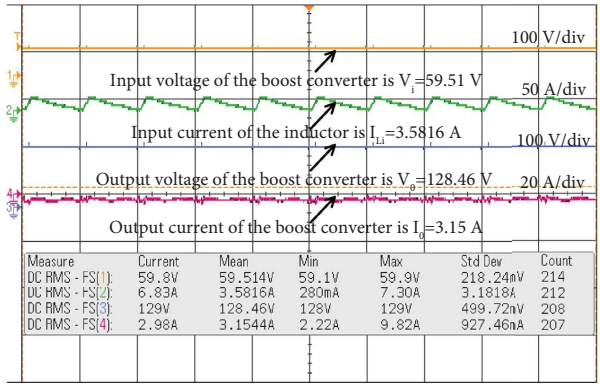

Figure 16: Supplied converter voltage parameters and current parameters at 0.1.

Table 7: Selected experimental parameters for testing the boost converter.

Variable	Specification
Utilized programming-based DC supply	M62012P8060
Utilized lamp load for testing converter	60 W
TLP-250 MOSFET gate driver circuit	0–5 V
Applied switching frequency for testing converter	20 kHz
MOSFET switch	IRF-640N
Optocoupler for TLP-250	4N25
Input capacitors are C_l, C_j, C_k, C_h, and C_g	20 μF
I/P and O/P inductors (L_q, and L_w)	20 μH

571.10 V, 5293.55 W, 9.27 A, 571.35 V, 5296.42 W, 9.281 A, 570.75 V, 5297.22 W, 9.30 A, 569.86 V, 5299.71 W, 9.312 A, 577.77 V, and 5380.21 W, respectively. The overall analysis of the proposed system is illustrated in Table 6.

7. Experimental Validation of the Proposed Converter

In this section, the proposed power converter is investigated for improving the load power rating of the overall system. Here, the selected power converter network is analyzed by considering the programming-based DC source device which is mentioned in Figure 14. From Figure 14, the 0–12 V transformer is used for reducing the source voltage from a higher level to a lower level to activate the TLP-250 MOSFET driver circuit. Here, the IRF-640 MOSFET device is selected for running the proposed converter under a continuous power supply mode of operation. The MOSFET features are high source impedance, less power absorption losses, more thermal stability, and more temperature withstanding ability. From Figure 14, the supply and load voltage and current parameters are determined by selecting the differential voltage and current meters. The selected switching device is protected by using the TLP-250 controller from the quick changes in supply voltages. The switching conditions of the MOSFET are optimized by interfacing with the analog discovery device. The MOSFET device receives the switching signals from the analog discovery device which is equal to 10%. The supplied voltage across the gate terminal of the MOSFET is 4.617 V and the current passing through the drain terminal is 1.8942 A as mentioned in Figure 15. From Figure 15, the drain voltage of the MOSFET is higher than the current passing through the device low and it attains high value when the switching voltage is low. The utilized input voltage for this converter is 59.51 V and it is enhanced to 128.46 V with a 10% duty cycle as shown in Figure 16. The overall setup design parameters are given in Table 7.

8. Conclusion

The overall GWAFC interfaced polymer membrane fuel stack system is developed by using the MATLAB software. Here, the polymer membrane fuel cell is selected because of its attractive features such as fast response, easy handling, ability to work in low as well as high-temperature conditions, more energy density, and simple construction. However, the fuel stack source voltage is very low which is not suitable for electric vehicle application. So, the new power DC-DC single switch converter is developed to enhance the system voltage to meet the required peak load demand. The advantages of this converter are a good voltage conversion ratio, fewer power components required for implementation, easy handling, wide output voltage operation, and suitable for all renewable energy system applications. Here, the duty signal of the converter is obtained by using the grey wolf optimization-based fuzzy logic power point tracking controller. In this MPPT controller, the fuzzy membership functions are selected by applying the grey wolf controller. The merits of this proposed MPPT controller are high flexibility, good dynamic response, easy handling, high robustness, and more reliability.

Data Availability

The data used to support the findings of this study are included within the article.

Conflicts of Interest

The authors declare that they have no conflicts of interest.

References

[1] Z. Chen, Q. Zhou, Y. Zhang, and X. Zhang, "Energy, exergy and economic (3E) evaluations of a novel power generation system combining supercritical water gasification of coal with chemical heat recovery," *Energy Conversion and Management*, vol. 276, 2023.

[2] M. Mahdavi, F. Jurado, R. A. V. Ramos, and A. Awaafo, "Hybrid biomass, solar and wind electricity generation in rural areas of Fez-Meknes region in Morocco considering water consumption of animals and anaerobic digester," *Applied Energy*, vol. 343, 2023.

[3] K. A. H. Al-Gburi, F. B. I. Alnaimi, B. A. J. Al-quraishi, E. S. Tan, and A. K. Kareem, "Enhancing savonius vertical Axis wind turbine performance: a comprehensive approach with numerical analysis and experimental investigations," *Energies*, vol. 16, no. 10, p. 4204, 2023.

[4] M. S. Moradi Ghareghani, A. Abdolahifar, and S. Karimian, "Numerical investigation on the helix angle to smoothen aerodynamic torque output of the 3-PB Darrieus vertical axis wind turbine," *Journal of Wind Engineering and Industrial Aerodynamics*, vol. 234, 2023.

[5] A. Kumbhar, N. Patil, M. Narule, S. M. Nadaf, and C. H. Basha, "Reducing grid dependency and operating cost of micro grids with effective coordination of renewable and electric vehicle's storage," *Soft Computing for Problem Solving: Proceedings of the SocProS 2022*, pp. 639–653, Springer Nature, Singapore, 2023.

[6] K. R. Reddy, C. H. Basha, V. Prashanth, C. Dhanamjayulu, S. Shivashimpiger, and R. Likhitha, "A novel on energy management strategy with maximum exploitation of renewables and EV storage in distribution networks," *International Transactions on Electrical Energy Systems*, vol. 2023, Article ID 1365608, 18 pages, 2023.

[7] T. Mariprasath, C. Shilaja, C. H. Hussaian Basha, M. Murali, F. Fathima, and S. Aisha, "Design and analysis of an improved artificial neural network controller for the energy efficiency enhancement of wind power plant," *Computational Methods and Data Engineering: Proceedings of ICCMDE 2021*, pp. 67–77, Springer Nature, Singapore, 2022.

[8] V. Udhay Sankar, C. H. Hussaian Basha, D. Mathew, C. Rani, and K. Busawon, "Application of wind-driven optimization for decision-making in economic dispatch problem," *Soft Computing for Problem Solving: SocProS*, Springer, Singapore, 2020.

[9] V. N. Dinh, P. Leahy, E. McKeogh, J. Murphy, and V. Cummins, "Development of a viability assessment model for hydrogen production from dedicated offshore wind farms," *International Journal of Hydrogen Energy*, vol. 46, no. 48, pp. 24620–24631, 2021.

[10] M. Li, H. Luo, S. Zhou et al., "State-of-the-art review of the flexibility and feasibility of emerging offshore and coastal ocean energy technologies in East and Southeast Asia," *Renewable and Sustainable Energy Reviews*, vol. 162, 2022.

[11] C. H. H. Basha and C. Rani, "Different conventional and soft computing MPPT techniques for solar PV systems with high step-up boost converters: a comprehensive analysis," *Energies*, vol. 13, no. 2, p. 371, 2020.

[12] C. H. Hussaian Basha and C. Rani, "Performance analysis of MPPT techniques for dynamic irradiation condition of solar PV," *International Journal of Fuzzy Systems*, vol. 22, no. 8, pp. 2577–2598, 2020.

[13] C. H. Hussaian Basha, V. Bansal, C. Rani, R. M. Brisilla, and S. Odofin, "Development of cuckoo search MPPT algorithm for partially shaded solar PV SEPIC converter," *Soft Computing for Problem Solving: SocProS*, Springer, Singapore, 2020.

[14] S. R. Kiran, C. H. Basha, V. P. Singh, C. Dhanamjayulu, B. R. Prusty, and B. Khan, "Reduced simulative performance analysis of variable step size ANN based MPPT techniques for partially shaded solar PV systems," *IEEE Access*, vol. 10, no. 2022, pp. 48875–48889, 2022.

[15] Z. Zakaria, S. K. Kamarudin, K. A. Abd Wahid, and S. H. Abu Hassan, "The progress of fuel cell for malaysian residential consumption: energy status and prospects to introduction as a renewable power generation system," *Renewable and Sustainable Energy Reviews*, vol. 144, 2021.

[16] C. H. Basha and C. Rani, "Design and analysis of transformerless, high step-up, boost DC-DC converter with an improved VSS-RBFA based MPPT controller," *International Transactions on Electrical Energy Systems*, vol. 30, no. 12, 2020.

[17] P. T. Bankupalli, S. Ghosh, L. Kumar, S. Samanta, and S. Jain, "Operational adaptability of PEM fuel cell for optimal voltage regulation with maximum power extraction," *IEEE Transactions on Energy Conversion*, vol. 35, no. 1, pp. 203–212, 2020.

[18] N. Lymperopoulos, D. Tsimis, A. Aguilo-Rullan, M. Atanasiu, E. Zafeiratou, and D. Dirmiki, "The status of SOFC and SOEC R&D in the European fuel cell and hydrogen joint undertaking programme," *ECS Transactions*, vol. 91, no. 1, pp. 9–26, 2019.

[19] I. A. Saleh, N. Zouari, and M. A. Al-Ghouti, "Removal of pesticides from water and wastewater: chemical, physical and biological treatment approaches," *Environmental Technology & Innovation*, vol. 19, 2020.

[20] A. L. J. Keow, W. Zuo, F. Ghorbel, and Z. Chen, "Reversible fuel cell enabled underwater buoyancy control," *Mechatronics*, vol. 86, 2022.

[21] T. Ferriday and P. H. Middleton, "Alkaline fuel cell technology-A review," *International Journal of Hydrogen Energy*, vol. 46, no. 35, pp. 18489–18510, 2021.

[22] W. A. Auriyani, D. Bustan, and S. Haryati, "The electrolyte-fuel concentrations effects on direct methanol alkaline fuel cell (DMAFC) through non-noble metal catalysts," *Journal of Science and Applicative Technology*, vol. 5, no. 1, pp. 25–29, 2021.

[23] N. M. Khoa, T. Sangeetha, P. T. Chen et al., "High performance zinc–air fuel cell with zinc particle fuel and flowing electrolyte," *Journal of the Chinese Institute of Engineers*, vol. 44, no. 8, pp. 842–850, 2021.

[24] R. C. Raimundo, J. V. Vargas, J. C. Ordonez et al., "A sustainable alkaline membrane fuel cell (SAMFC) stack characterization, model validation and optimal operation," *International Journal of Hydrogen Energy*, vol. 45, no. 9, pp. 5723–5733, 2020.

[25] F. Destyorini, W. C. Amalia, Y. Irmawati et al., "High graphitic carbon derived from coconut coir waste by promoting potassium hydroxide in the catalytic graphitization process

for lithium-ion battery anodes," *Energy & Fuels*, vol. 36, no. 10, pp. 5444–5455, 2022.

[26] P. Murugan, "Implement using KY converter for hybrid renewable energy applications: design, analysis, and implementation," *Advanced Statistical Modeling, Forecasting, and Fault Detection in Renewable Energy Systems*, IntechOpen, London, UK, 2020.

[27] A. Mehta, R. A. Rather, B. Belec, S. Gardonio, M. Fang, and M. Valant, "Plastic waste precursor-derived fluorescent carbon and construction of ternary FCs@ CuO@ TiO2 hybrid photocatalyst for hydrogen production and sensing application," *Energies*, vol. 15, no. 5, p. 1734, 2022.

[28] Q. Sun, D. Lin, M. Khayatnezhad, and M. Taghavi, "Investigation of phosphoric acid fuel cell, linear Fresnel solar reflector and Organic Rankine Cycle polygeneration energy system in different climatic conditions," *Process Safety and Environmental Protection*, vol. 147, pp. 993–1008, 2021.

[29] L. P. R. Nadimuthu, K. Victor, C. H. Basha et al., "Energy conservation approach for continuous power quality improvement: a case study," *IEEE Access*, vol. 9, no. 2021, pp. 146959–146969.

[30] C. H. Basha and M. Murali, "A new design of transformerless, non-isolated, high step-up DC-DC converter with hybrid fuzzy logic MPPT controller," *International Journal of Circuit Theory and Applications*, vol. 50, no. 1, pp. 272–297, 2022.

[31] M. Büyük and M. İnci, "Improved drift-free P&O MPPT method to enhance energy harvesting capability for dynamic operating conditions of fuel cells," *Energy*, vol. 267, 2023.

[32] N. Karami, L. El Khoury, G. Khoury, and N. Moubayed, "Comparative study between P&O and incremental conductance for fuel cell MPPT," in *Proceedings of the International Conference on Renewable Energies for Developing Countries 2014*, IEEE, Beirut, Lebanon, November 2014.

[33] Shashikant and B. Shaw, "Comparison of SCA-optimized PID and P&O-based MPPT for an off-grid fuel cell system," *Soft Computing in Data Analytics: Proceedings of International Conference on SCDA 2018*, Springer, Singapore, 2019.

[34] M. İnci, "A flexible perturb & observe MPPT method to prevent surplus energy for grid-failure conditions of fuel cells," *International Journal of Hydrogen Energy*, vol. 46, no. 79, pp. 39483–39498, 2021.

[35] P. Y. Chen, K. N. Yu, H. T. Yau, J. T. Li, and C. K. Liao, "A novel variable step size fractional order incremental conductance algorithm to maximize power tracking of fuel cells," *Applied Mathematical Modelling*, vol. 45, pp. 1067–1075, 2017.

[36] J. Hahm, H. Kang, J. Baek, H. Lee, and M. Park, "Design of incremental conductance sliding mode MPPT control applied by integrated photovoltaic and proton exchange membrane fuel cell system under various operating conditions for BLDC motor," *International Journal of Photoenergy*, vol. 2015, Article ID 828129, 14 pages, 2015.

[37] N. Priyadarshi, S. Padmanaban, P. Kiran Maroti, and A. Sharma, "An extensive practical investigation of FPSO-based MPPT for grid integrated PV system under variable operating conditions with anti-islanding protection," *IEEE Systems Journal*, vol. 13, no. 2, pp. 1861–1871, 2019.

[38] N. Priyadarshi, M. S. Bhaskar, P. Sanjeevikumar, F. Azam, and B. Khan, "High-power DC-DC converter with proposed HSFNA MPPT for photovoltaic based ultra-fast charging system of electric vehicles," *IET Renewable Power Generation*, pp. 1–13, 2022.

[39] N. Priyadarshi, P. Sanjeevikumar, M. S. Bhaskar, F. Azam, I. B. Taha, and M. G. Hussien, "An adaptive TS-fuzzy model based RBF neural network learning for grid integrated photovoltaic applications," *IET Renewable Power Generation*, vol. 16, no. 14, pp. 3149–3160, 2022.

[40] N. Priyadarshi, S. Padmanaban, M. S. Bhaskar, and B. Khan, "An experimental performance verification of continuous mixed P-norm based adaptive asymmetrical fuzzy logic controller for single stage photovoltaic grid integration," *IET Renewable Power Generation*, 2022.

[41] N. Priyadarshi, P. K. Maroti, and B. Khan, "An adaptive grid integrated photovoltaic system with perturb T–S fuzzy based sliding mode controller MPPT tracker: an experimental realization," *IET Renewable Power Generation*, 2023.

[42] N. Priyadarshi, S. Padmanaban, M. S. Bhaskar, F. Azam, B. Khan, and M. G. Hussien, "A novel hybrid grey wolf optimized fuzzy logic control based photovoltaic water pumping system," *IET Renewable Power Generation*, 2022.

[43] Y. H. Li, S. S. Choi, and S. Rajakaruna, "An analysis of the control and operation of a solid oxide fuel-cell power plant in an isolated system," *IEEE Transactions on Energy Conversion*, vol. 20, no. 2, pp. 381–387, 2005.

[44] L. Zhang, W. Tang, F. Wang, C. Xie, W. Zhou, and H. Xie, "Optimization and control for solid oxide fuel cell system hybrid DC microgrids from the perspective of high efficiency, thermal safety, and transient response," *Frontiers in Energy Research*, vol. 10, 2022.

[45] C. Wang and M. Nehrir, "Short-time overloading capability and distributed generation applications of solid oxide fuel cells," *IEEE Transactions on Energy Conversion*, vol. 22, no. 4, pp. 898–906, 2007.

[46] H. Masuda, K. Yada, and A. Osaka, "Self-ordering of cell configuration of anodic porous alumina with large-size pores in phosphoric acid solution," *Japanese Journal of Applied Physics*, vol. 37, p. L1340, 1998.

[47] H. Rezk and A. Fathy, "Performance improvement of PEM fuel cell using variable step-size incremental resistance MPPT technique," *Sustainability*, vol. 12, no. 14, p. 5601, 2020.

[48] B. Kanouni and S. Mekhilef, "A SMC-based MPPT controller for proton exchange membrane fuel cell system," in *Proceedings of the 2022 19th International Multi-Conference on Systems, Signals & Devices (SSD)*, Sétif, Algeria, May 2022.

[49] J. C. Rosas-Caro, P. M. García-Vite, A. Rodríguez et al., "Differential evolution based algorithm for optimal current ripple cancelation in an unequal interleaved power converter," *Mathematics*, vol. 9, no. 21, p. 2755, 2021.

[50] S. JemeÏJemei, D. Hissel, M. C. PéraPera, and J. M. Kauffmann, "A new modeling approach of embedded fuel-cell power generators based on artificial neural network," *IEEE Transactions on Industrial Electronics*, vol. 55, no. 1, pp. 437–447, 2008.

[51] A. U. Chávez-Ramírez, R. Muñoz-Guerrero, S. M. Durón-Torres et al., "High power fuel cell simulator based on artificial neural network," *International Journal of Hydrogen Energy*, vol. 35, no. 21, pp. 12125–12133, 2010.

[52] S. Jemëi, D. Hissel, M. C. Péra, and J. M. Kauffmann, "On-board fuel cell power supply modeling on the basis of neural network methodology," *Journal of Power Sources*, vol. 124, no. 2, pp. 479–486, 2003.

[53] C. Hussaian Basha, T. Mariprasath, M. Murali, and S. Rafikiran, "Simulative design and performance analysis of hybrid optimization technique for PEM fuel cell stack based EV application," *Materials Today: Proceedings*, vol. 52, pp. 290–295, 2022.

[54] B. Karthikeyan, D. Karthikeyan, V. P. Arumbu, K. Sundararaju, R. Palanisamy, and P. Divya, "A feed-forward neural network based MPPT controller for PEMFC system

with ultra high step up converter," in *Proceedings of International Conference on Power Electronics and Renewable Energy Systems: ICPERES 2021*, Springer Singapore, Chennai, India, November 2022.

[55] A. A. M. Nureddin, J. Rahebi, A. Ab-BelKhair, and A. Ab-BelKhair, "Power management controller for microgrid integration of hybrid PV/fuel cell system based on artificial deep neural network," *International Journal of Photoenergy*, vol. 2020, Article ID 8896412, 21 pages, 2020.

[56] S. R. Kiran, C. H. Basha, A. Kumbhar, and N. Patil, "A new design of single switch DC-DC converter for PEM fuel cell based EV system with variable step size RBFN controller," *Sādhanā*, vol. 47, no. 3, p. 128, 2022.

[57] T. Hai, D. Wang, and T. Muranaka, "An improved MPPT control-based ANFIS method to maximize power tracking of PEM fuel cell system," *Sustainable Energy Technologies and Assessments*, vol. 54, 2022.

[58] M. S. Abou Omar, H. J. Zhang, Y. X. Su, and Y. X. Su, "Fractional order fuzzy PID control of automotive PEM fuel cell air feed system using neural network optimization algorithm," *Energies*, vol. 12, no. 8, p. 1435, 2019.

[59] C. H. H. Basha and C. Rani, "A New single switch DC-DC converter for PEM fuel cell-based electric vehicle system with an improved beta-fuzzy logic MPPT controller," *Soft Computing*, vol. 26, no. 13, pp. 6021–6040, 2022.

[60] S. Rafikiran, G. Devadasu, C. H. Basha et al., "Design and performance analysis of hybrid MPPT controllers for fuel cell fed DC-DC converter systems," *Energy Reports*, vol. 9, pp. 5826–5842, 2023.

[61] C. Hähnel, V. Aul, and J. Horn, "Power control for efficient operation of a PEM fuel cell system by nonlinear model predictive control," *IFAC-PapersOnLine*, vol. 48, no. 11, pp. 174–179, 2015.

[62] C. H. Basha, S. Rafikiran, M. Narule et al., "Design and analysis of genetic algorithm optimization-based ANFIS controller for interleaved DC-DC converter-fed PEMFC system," *Congress on Intelligent Systems*, Springer Nature, Singapore, 2022.

[63] C. H. Basha, M. Murali, T. Mariprasanth, S. Rafikiran, and F. Fathima, "Design and analysis of an adaptive soft computing power point tracing techniques for time-varying irradiation condition of solar PV," *Computer Vision and Robotics: Proceedings of CVR 2021*, pp. 381–392, Springer, Singapore, 2022.

[64] A. Dahbi, N. Nait-Said, and M. S. Nait-Said, "A novel combined MPPT-pitch angle control for wide range variable speed wind turbine based on neural network," *International Journal of Hydrogen Energy*, vol. 41, no. 22, pp. 9427–9442, 2016.

[65] M. Murali, S. Rafi Kiran, C. H. Hussaian Basha, S. Khaja Khizar, and P. M. Preethi Raj, "Design of high step-up interleaved boost converter-fed fuel cell-based electric vehicle system with neural network controller," *Pattern Recognition and Data Analysis with Applications*, pp. 789–801, Springer Nature, Singapore, 2022.

[66] S. S. Patil, B. S. Varma, G. Devadasu, C. H. Basha, M. J. R. Inamdar, and S. S. Salman, "Performance analysis of image caption generation using deep learning techniques," in *Proceedings of the International Conference on Microelectronic Devices, Circuits and Systems*, Springer Nature Switzerland, Vellore, India, August 2022.

[67] G. Xu, Z. Yu, L. Xia, C. Wang, and S. Ji, "Performance improvement of solid oxide fuel cells by combining three-dimensional CFD modeling, artificial neural network and genetic algorithm," *Energy Conversion and Management*, vol. 268, 2022.

[68] S. Bozorgmehri and M. Hamedi, "Modeling and optimization of anode-supported solid oxide fuel cells on cell parameters via artificial neural network and genetic algorithm," *Fuel Cells*, vol. 12, no. 1, pp. 11–23, 2012.

[69] P. Tian, X. Liu, K. Luo, H. Li, and Y. Wang, "Deep learning from three-dimensional multiphysics simulation in operational optimization and control of polymer electrolyte membrane fuel cell for maximum power," *Applied Energy*, vol. 288, 2021.

[70] M. Amirabadi and S. Farhangi, "Fuzzy control of hybrid fuel cell/battery power source in electric vehicle," in *Proceedings of the 2006 1ST IEEE Conference on Industrial Electronics and Applications*, Singapore, May 2006.

[71] A. Harrag and H. Rezk, "Indirect P&O type-2 fuzzy-based adaptive step MPPT for proton exchange membrane fuel cell," *Neural Computing & Applications*, vol. 33, no. 15, pp. 9649–9662, 2021.

[72] A. Harrag and S. Messalti, "How fuzzy logic can improve PEM fuel cell MPPT performances?" *International Journal of Hydrogen Energy*, vol. 43, no. 1, pp. 537–550, 2018.

[73] H. Reddy, S. Sharma, and S. R. K. K, "Implementation of adaptive neuro fuzzy controller for fuel cell based electric vehicles," *Gazi University Journal of Science*, vol. 34, no. 1, pp. 112–126, 2021.

[74] J. M. Correa, F. A. Farret, and L. N. Canha, "An analysis of the dynamic performance of proton exchange membrane fuel cells using an electrochemical model," in *Proceedings of the IECON'01. 27th Annual Conference of the IEEE Industrial Electronics Society (Cat. No. 37243)*, IEEE, Denver, CO, USA, November 2001.

[75] N. Bigdeli, "Optimal management of hybrid PV/fuel cell/battery power system: a comparison of optimal hybrid approaches," *Renewable and Sustainable Energy Reviews*, vol. 42, pp. 377–393, 2015.

[76] F. Evran and M. T. Aydemir, "Z-source-based isolated high step-up converter," *IET Power Electronics*, vol. 6, no. 1, pp. 117–124, 2013.

[77] Z. Jiang and R. A. Dougal, "Synergetic control of power converters for pulse current charging of advanced batteries from a fuel cell power source," *IEEE Transactions on Power Electronics*, vol. 19, no. 4, pp. 1140–1150, 2004.

[78] A. J. Sabzali, E. H. Ismail, and H. M. Behbehani, "High voltage step-up integrated double Boost–Sepic DC–DC converter for fuel-cell and photovoltaic applications," *Renewable Energy*, vol. 82, pp. 44–53, 2015.

[79] J.-Y. Lee, Y. S. Jeong, and B.-M. Han, "An isolated DC/DC converter using high-frequency unregulated $ LLC $ resonant converter for fuel cell applications," *IEEE Transactions on Industrial Electronics*, vol. 58, no. 7, pp. 2926–2934, 2011.

[80] S. Farhani, A. N'Diaye, A. Djerdir, and F. Bacha, "Design and practical study of three phase interleaved boost converter for fuel cell electric vehicle," *Journal of Power Sources*, vol. 479, 2020.

[81] H. B. Ch, C. Dhanamjayulu, I. Kamwa, I. Kamwa, and S. Muyeen, "A novel on intelligent energy control strategy for micro grids with renewables and EVs," *Energy Strategy Reviews*, vol. 52, 2024.

[82] V. Prashanth, S. Rafikiran, C. H. Hussaian Basha et al., "Implementation of high step-up power converter for fuel cell application with hybrid MPPT controller," *Scientific Reports*, vol. 14, no. 1, p. 3342, 2024.